International Journal of Heat and Mass Transfer 203 (2023) 123813

Contents lists available at ScienceDirect

International Journal of Heat and Mass Transfer

journal homepage: www.elsevier.com/locate/hmt

Experimental investigation, CFD and theoretical modeling of two-phase heat transfer in a three-leg multi-channel heat pipe

Valentin Guichet[a], Bertrand Delpech[a], Hussam Jouhara[a,b,*]

[a] Heat Pipe and Thermal Management Research Group, College of Engineering, Design and Physical Sciences, Brunel University London, UB8 3PH, United Kingdom

[b] Vytautas Magnus University, Studentu Str. 11, Kaunas Distr., Akademija LT-53362, Lithuania

ARTICLE INFO

Article history:
Received 25 November 2022
Revised 24 December 2022
Accepted 25 December 2022
Available online 30 December 2022

Keywords:
Heat pipe
Multi-leg heat pipe
Two phase heat transfer
CFD modelling

ABSTRACT

Muti-channel flat heat pipe is an innovative technology recently used at the rear of photovoltaic cells to absorb and reuse the wasted heat. To better understand the fundamentals of two-phase heat transfer (boiling and condensation) taking place inside multi-channel heat pipes, a unique three-leg heat pipe has been built. This one-of-a-kind heat pipe was used to develop both computational fluid dynamic (CFD) and theoretical models of a multi-channel heat pipe. To simulate the heat pipe operation with ANSYS Fluent, the Volume of Fluid (VOF) approach and Lee model were investigated. Different types of Lee models using user defined function (UDF) were compared and the influence of the condenser's boundary condition, saturation temperature, and mass transfer coefficient on the simulations was studied. For the first time, major limits of the Lee model for the simulation of heat pipes are identified. It is concluded that the available Lee model cannot predict the heat pipe temperature as it shows low physical meaning and can easily be manipulated to adjust the simulation's results. Based on the three-leg heat pipe experimental data, a new multi-channel theoretical model was developed that uses the thermal-electrical resistance analogy to predict the three-leg heat pipe thermal resistance. By selecting the optimum correlations for pool boiling and filmwise condensation, the developed iterative theoretical model was able to predict the three-leg heat pipe thermal resistance with an error of 8.2%.

1. Introduction

In the objective of maintaining an optimum temperature of photovoltaic (PV) cells and batteries, multi-channel flat heat pipes have been used for cooling purposes [1–6]. In addition to cooling down the photovoltaic panels and thus providing a high electrical production, the thermal absorber allows a simultaneous production of thermal energy. If such heat pipes have been tested experimentally, their modelling using computational fluid dynamic (CFD) software and theory approach remain tedious and important progress must be done to predict their performances with CFD or theoretical approaches.

1.1. Numerical (CFD) modelling of multi-channel heat pipe – state of the art

The CFD simulation of heat pipes has received extensive attention in the past 20 years. Multi-phase flows as occurring in heat pipes are tedious to simulate as it requires the partitioning of the domain in subdomains for each phase, and the addition of source terms to the Navier-Stokes transport equations. For the introduction of source terms which describes the mass and heat transfer taking place during a liquid-vapour phase change process, four main models are available: the Schrage [7], Lee [8], Wang et al. [9], and Nichita and Thome [10] models. Legierski et al. [11] also used the Hertz-Knudsen [12] model to simulate a horizontal wicked heat pipe. A C-based user defined function (UDF) was codded to calculate the source terms. The evaporation coefficient was adjusted between 0.01 s^{-1} and 0.0001 s^{-1} to fit the experimental data. However, the conducted simulation was semi-empirical and did not success into modelling boiling and condensation. Wang et al. [9] developed a model based on the Hertz-Knudsen [12] equation. This model was expressed in terms of pressure so that the impact of hydrostatic pressure on the boiling pat-

* Corresponding author at: Heat Pipe and Thermal Management Research Group, College of Engineering, Design and Physical Sciences, Brunel University London, UB8 3PH, United Kingdom.
E-mail address: hussam.jouhara@brunel.ac.uk (H. Jouhara).

https://doi.org/10.1016/j.ijheatmasstransfer.2022.123813

Nomenclature

A	surface area m^2
c_p	specific heat J.kg^{-1}.K^{-1}
D	diameter m
g	gravitational acceleration m.s^{-2}
h	heat transfer coefficient W.m^{-2}.K^{-1}
i_{lv}	latent heat of vaporization J.kg^{-1}
k	thermal conductivity W.m^{-1}.K^{-1}
L	length m
$\dot{m}$	mass flow rate kg.s^{-1}
P	pressure Pa
Pr	Prandtl number, ($Pr = \mu c_p/k$) Dimensionless
$\dot{Q}$	heat transfer rate W
q''	heat flux per surface unit area W.m^{-2}
R	thermal resistance K.W^{-1}
T	temperature K

Greek symbols

Δ	difference
Γ	mass rate of liquid flow per unit periphery kg.m^{-1}.s^{-1}
ρ	density kg.m^{-3}
σ	surface tension N.m^{-1}
μ	dynamic viscosity Pa.s

Subscripts

Alum	aluminium
atm	atmospheric
ax	axial
boiling	boiling
c	condenser /
condensation	condensation
e	evaporator
ffb	falling film boiling
i	inner
in	inlet
pb	pool boiling
o	outer
out	outlet
s	surface
sat	saturation
v	vapour
w	Wall

Superscripts

"	per surface area m^{-2}
.	per unit of time s^{-1}
*	dimensionless dimensionless

Acronyms

FR	filling ratio
HP	heat pipe
PV/T	photovoltaic/thermal
VOF	volume of fluid

tern was considered. This model was used to model a 54 m long thermosyphon with four different filing ratios. The initial height of the liquid pool was set to 5 m, 10 m, 20 m, and 40 m. It was observed that, at the bottom of the simulated thermosyphon, no bubbles are forming. Most of the bubbles are formed near the surface and the higher the bubbles in the liquid pool, the larger the bubbles. At the condenser section, the formation of a liquid condensate was observed. At the upper section of the condenser, due to the condensing vapour, liquid droplets were forming near the wall. At the lower part of the condenser, the droplets merge and form a liquid film. Unfortunately, Wang et al. [9] did not compare their simulation to experimental data. Temimy and Abdulrasool [13] simulated a thermosyphon at various heat transfer rates in the range 20–120 W. The objective of the authors was to numerically study the interactions between the steam and condensate. Unfortunately, the source terms used for the simulation carried out was not reported. The work from Temimy and Abdulrasool [13] can be criticized as the heat pipe operation was not successfully simulated. Instead of having rising vapour in the core of the heat pipe and a liquid condensate near the wall, both phases were flowing near the wall. According to the authors, the liquid and vapour phases interact with each other and would push the phase with lower momentum to the centre of the thermosyphon. Yet, this disagrees with the commonly accepted two-phase working cycle of a thermosyphon. Moreover, this simulation was not compared to experiments. It is therefore concluded that the simulation from Temimy and Abdulrasool [13] was unsuccessful. Recently, Wang et al. [14] used CFD simulations to investigate the effects of hydrogen permeation on the heat transfer performance of liquid metal heat pipes. To account for the superheat needed for nucleation and the influence of pressure variation inside the heat pipe, Wang et al. [14] used a modified version of the Lee [8] model by expressing the source terms in terms of pressure. Based on the temperature of the simulated heat pipe, the authors considered the model to accurately represent the experiments. However, high experimental uncertainties are observed in the temperature measurements with temperature variations as high as 200 °C between several thermocouples located at the condenser. Moreover, the Volume of Fluid contours of the simulated heat pipe reveals a rapid degradation of the liquid pool which disappears. This cannot occur in a real heat pipe and would automatically generate a dry out of the evaporator that would prevent the good operation of the heat pipe. In terms of temperature, the simulated contours shows that the heat transfer inside the heat pipe is mainly caused by the projection of liquid geysers from the evaporator to the condenser. The evaporator temperature mainly increases due to the evaporator dryout and is expected to increase to much higher values if the operation of the heat pipe was simulated for more than 100 s. Hence, concerns can be raised on the successful CFD simulation of the liquid metal heat pipe made by Wang et al. [14]. In 2022, Sun et al. [15] used STAR-CCM+ to simulate heat pipes and the effect of the orientation on the thermal performance. The Volume of Fluid approach was used to differentiate the liquid and vapour phases. To simplify the simulation and improve its feasibility, the phase change process was chosen not to be modelled. Instead, to model boiling and condensation, extremely large thermal conductivities were implemented for the liquid and vapour phases. The root-mean-square deviation between the CFD and experiment was about 15%. However, the oversimplification of the boiling and condensation phenomena in the conducted CFD simulation is a major limit. As boiling and condensation are not simulated, the impact of the angle on the two-phase heat transfer cannot be accurate. Indeed, pool boiling and filmwise condensation have a very specific behaviour while changing the heat pipe tilt angle which cannot be reproduced without simulation the boiling activity.

In the available Euler-Euler approaches which are suitable for heat pipe simulations, the Volume of Fluid technique is largely preferred for its capacity to track bubbles and droplets. Out of twenty reviewed works on heat pipe simulation, to simulate the two-phase cycle inside heat pipes, fourteen reported the use of the Lee [8] model [16–29]. In 2010, the work from Alizadehdakhel et al. [16] was one of the first reporting a comparison between a heat pipe simulation and experimental data. The conducted simulation was a 2D thermosyphon and was simulated using the Lee [8] model. The saturation temperature was set to 350K, and the mass transfer coefficients were kept at their default values of

0.1 s^{-1}. The simulation was compared to temperature measurements from a 1m long thermosyphon tested at heat transfer rates of 350 W, 500 W, and 700 W. In the simulation, both pool boiling and filmwise condensation were observed. The falling film returning to the evaporator's pool was observed. The temperature difference between the simulation and experiments at the evaporator and condenser were 0.9 °C and 5.4 °C. However, the temperature discrepancy was high at the adiabatic section. Indeed, a difference of temperature of 16 °C was observed at the adiabatic section. This difference of temperature was assumed by the authors to be caused by thermal losses during the experiments. Lin et al. [17] simulated a miniature oscillating heat pipe using the Volume of Fluid (VOF) approach and Lee [8] model. A user defined function was codded for the implementation of the source terms. According to the authors, the mixture model was more adapted for the simulation of an oscillating heat pipe due to the moving slugs of vapour. The saturation temperature input was set by the authors to 303 K and was taken from the experiments. For the validation, Lin et al. [17] used a semi-transparent oscillating heat pipe. However, Lin et al. [17] did not show the volume of fluid contours from their simulation. Indeed, the fluid dynamic was not presented which raises doubts on the success of the simulation carried out. A temperature comparison between the simulation and the experiments reports that the temperature difference at the evaporator was 8.9 °C whereas, at the condenser, the temperature difference was 4.8 °C. Among the works using the Lee [8] model for the simulation of heat pipes, Fadhl et al. [21,30] is considered as a reference. The authors presented the 2D simulation of a thermosyphon using water, R134a, and R404a with the Lee [8] model. The authors mentioned that the included Lee model of CFD software was unable to simulate boiling and condensation and that C codded user-defined-functions (UDFs) were required. The mass transfer coefficients were kept to 0.1 s^{-1}. However, the input saturation temperature was not reported. Fadhl et al. [21,30] successfully presented contours from the simulation showing the boiling and condensation of the working fluid. Moreover, the simulation clearly shows the transient warmup of the simulated thermosyphon. For their simulation, the difference of temperature between the simulation and experimental data was in the range of 15 °C at the evaporator, 5 °C at the adiabatic section, and 4 °C at the condenser. Asmaie et al. [20] simulated a CuO/water nanofluid thermosyphon using the Lee [8] model. The mass transfer coefficient was kept to 0.1 s^{-1}. The authors set constant heat flux conditions for both evaporator and condenser's wall. In total, 450 s of thermosyphon's operation was simulated. The condenser contours showed that condensation took place. A liquid condensate returning to the evaporator was simulated. However, Asmaie et al. [20] did not show boiling contours. The simulation was compared to experimental data from Liu et al. [31] and the temperature difference between the simulation and the experiments were 5.1 °C at the evaporator, 0.3 °C at the adiabatic section, and 1.5 °C at the condenser. Fertahi et al. [32] also simulated a thermosyphon with fins at the condenser using the Volume of Fluid and Lee [8] model. The saturation temperature was set to 373 K. An important boiling activity was observed at the evaporator whereas, at the condenser, condensation takes place. However, in this simulation, condensation mainly appeared under the form of droplets. Yue et al. [24] simulated the evaporator section of a microchannel separate heat pipe. R22 was used as a working fluid inside copper microchannels. The Lee [8] model was implemented for the two-phase source terms. Yet, Yue et al. [24] admitted that the evaporation and condensation mass transfer coefficients were adapted to match the experimental measurements. The impact of the filling ratio on the thermal performance was studied numerically and the temperature difference between the simulation and the experiments obtained was 0.68 °C. Hosseinzadeh et al. [25] investigated the impact of a super-hydrophobic coating on the thermal performance of a heat pipe using both experimental and numerical techniques. The simulation was conducted using the Volume of Fluid and Lee [8] model. The mass transfer coefficients were set to their default value of 0.1 s^{-1}. The heat transfer rate studied was 250W. The volume of fluid contours revealed a surprising behaviour of the working fluid. Indeed, the simulated liquid pool region seems to explode. It is therefore doubtful that the simulation successfully simulated the operation of a thermosyphon. In 2022, Höhne [33] tried to simulate a heat pipe using the Lee [8] model source terms but coupled with homogeneous model instead of the commonly used Volume of Fluid approach. The source terms were introduced to the solver using a user-defined function. At the condenser, a constant temperature boundary condition was set on the wall. This boundary condition is wrong as it forces the simulation to converge to the condenser temperature indicated which was taken from experiments. Furthermore, the experimental results reveal that the CFD simulation of the heat pipe was a failure. To start with, the temperature of the adiabatic section of the heat pipe decreases with time. No heat transfer can be seen in the temperature contours of the simulated heat pipe. Furthermore, the pool boiling mechanism was not successfully simulated. Instead, the overall liquid pool volume evaporates but bubbles cannot be visualized. This is a common issue in the simulation of the heat pipe and reveals that the homogeneous model used by Höhne [33] is not suitable for the simulation of heat pipes.

An important factor in the implementation of the Lee [8] model is the value of the evaporation and condensation mass transfer coefficients. Alizadehdakhel et al. [16], Fadhl et al. [30], Asmaie et al. [20], and Hosseinzadeh et al. [25] all used the Lee [8] model source terms to simulate heat pipes and, to describe the mass transfer during evaporation and condensation, implemented a mass transfer coefficient of β=0.1 s^{-1}. Such input for the Lee [8] model was reported by the authors as suitable to simulate heat pipes. However, in the literature, other values of mass transfer coefficient were reported. If the evaporation mass transfer coefficient is usually kept to β_e=0.1 s^{-1}, Wang et al. [23] used a condensation mass transfer coefficient of β_c=110 s^{-1} whereas Tarokh et al. [28] proposed $\beta_c = \beta_e(\rho_l / \rho_v)$. Kafeel and Turan [19] also investigated the value of the condenser mass transfer coefficient. The authors proposed an equation to calculate the condenser mass transfer coefficient based on the evaporation heat transfer coefficient. Indeed, it seems that the value of the mass transfer coefficient has a significant impact on the simulation results. This was further highlighted by the study from Kim et al. [22] who investigated three different values for the condensation mass transfer coefficient. It was shown that the simulated condenser temperature increases with an increase of the condensation mass transfer coefficient.

In the literature, the use of the Lee [8] model for the simulation of a multi-channel heat pipe has not been covered to date. Furthermore, the versatility of the Lee [8] model and the influence of various factors such as saturation temperature, boundary condition, and mass transfer coefficient on the simulation results must be further studied to confirm the suitability of the Lee [8] model to numerically simulate heat pipes. For the first time, the CFD simulation of a unique three-leg multi-channel heat pipe has revealed major limits of the Lee [8] model which are identified and clearly reported in this work.

1.2. Theoretical modelling of multi-channel heat pipe-state of the art

In the literature, the number of theoretical models for multi-channel heat pipes is low. Almahmoud and Jouhara [34,35] developed a multi-channel heat pipe for waste heat recovery in the steel industry. The multi-channel heat pipe was made from 14 parallel stainless-steel tubes connected at the top and bottom by horizontal

collectors. A theoretical model was proposed to predict the thermal performance of the multi-channel heat pipe. This model was based on a thermal resistance network which includes the radiation thermal resistance and the heat pipe thermal resistance. For heat transfer rates in the range 4500 W–8500 W, the heat transfer rate was predicted with an average error of 14.3%. The heat pipe temperatures were predicted within an error of 3 °C. Delpech et al. [36] designed a multi-channel heat pipe used to recover thermal energy during the cooling of ceramic tiles. The multi-channel heat pipe was manufactured from stainless-steel. Ten parallel tubes were linked at the top and bottom by collectors to allow the circulation of the working fluid in the parallel channels. The authors developed a model based on a thermal resistance network to predict the heat transfer rate absorbed by the heat pipe and the heat pipe temperatures. The radiation thermal resistance of the kiln was modelled and, at heat transfer rates between 470 W and 2435 W, the theoretical model was able to predict the heat pipe thermal performance with an error lower than 7.5%. To date, Almahmoud and Jouhara [34,35] and Delpech et al. [36] are the only authors who proposed theoretical models of multi-channel heat pipes. In both case, the modelled multi-channel heat pipes consisted of parallel cylindrical stainless-steel tubes. Yet, in their models, the authors considered an equivalent heat transfer area of boiling and condensation and thus, assumed a constant temperature between each leg and the collectors. Recently, Guichet et al. [37,38] investigated the thermal performance of a multi-channel flat heat pipe and proposed a thermal resistance network which considers the multi-channel geometry. Heat transfer rates in the range 0–1500 W were investigated and the theoretical model accuracy was studied while determining the boiling, condensation, and total thermal resistance of a multi-channel heat pipe. By selecting optimum pool boiling and condensation correlations, the boiling and condensation thermal resistances were predicted within 17.2% and 14.4% of error, respectively. Overall, the multi-channel flat heat pipe thermal resistance was predicted with an average error of 13.1%. Yet, in this work, temperature measurements were taken from the flat surface of the heat pipe only and the temperature of each channel could not be studied independently. This limited the validation of the proposed model.

In this regard, to complete the work by Guichet et al. [37,38] and further validate the proposed multi-channel heat pipe thermal resistance network, the three-leg heat pipe prototype is used to study each parallel leg independently. The developed prototype permitted to monitor the local temperature of each leg and collector. These local temperature measurements were compared to the multi-channel thermal resistance network for validation. Finally, the multi-channel thermal resistance model was integrated to an iterative tool which was used to predict the thermal performance of the three-leg heat pipe.

2. Experimental apparatus

In the objective of studying two-phase heat transfer in a multi-channel geometry, a three-leg heat pipe prototype was designed and manufactured. The three-leg heat pipe is made from three parallel stainless-steel tubes with 6mm internal diameter. The three parallel channels are linked at the bottom and top by horizontal collectors. Those collectors allow the circulation of the working fluid in all the parallel channels. In this experiment, R134a was selected as a working fluid with a filling ratio of 50%. At the contact of a heat source, the saturated liquid pool boils at the evaporator and generates vapour. This vapour stream rises in the three parallel legs and condenses at the top of the three-leg heat pipe. Finally, the condensate returns to the evaporator under the action of gravity. The heat transfer principle of the three-leg heat pipe and the manufactured three-leg heat pipe prototype are shown in Fig. 1.

To investigate the two-phase heat transfer inside the three-leg heat pipe, a heat source and heat sink were needed. To ease the development of the numerical and theoretical models, constant temperature boundary conditions on the outer evaporator and condenser wall were chosen. To do so, phase change must take place outside of the three-leg heat pipe wall. As a heat source, it was therefore decided to use steam that condenses outside of the three-leg heat pipe evaporator's wall. To guarantee a uniform temperature of the three-leg heat pipe condenser wall, the condenser was immersed in a saturated pool of water. Pressurized cylinders were used around the three-leg heat pipe evaporator and condenser to provide the condensing steam and boiling water pool. Those cylinders were first vacuumed to avoid the introduction of non-condensable gases and then charged with saturated water under suitable temperature/pressure equilibrium. At the top of the three-leg heat pipe, a coil inside which cold water circulates was used to extract the heat from the system. The complete three-leg heat pipe assembly and its working principle are presented in Fig. 2.

At the bottom cylinder, two Omega 2-Piece Mica Insulated Band Heater of 800W each have been used and were electrically controlled. For this experiment, heat transfer rates in the range 0-110W were investigated with an incremental step of 10 W. The cooling water flow rate was kept at 1L/min and was measured manually by recovering a given volume of water in 10 s. The electrical consumption from the heaters were recorded with a power logger PEL 105. The steady state temperatures were recorded using a National Instrument datalogger with two NI-9213 thermocouples modules. To investigate the performances of the three-leg heat pipe, K-type thermocouples were welded on the stainless-steel wall. Two-thermocouples L1 and R1 are placed on the top collector in the condenser section. The thermocouples L2, M2, and R2 are placed on the left, middle, and right legs at the condenser's section. The thermocouples L3, M3, and R3 recorded the adiabatic section temperature of the three-leg heat pipe. As for the evaporator, the thermocouples L4, M4, R4 and L5, M5, R5 were placed on the legs whereas the thermocouples L6 and R6 were placed on the bottom collector. The three-leg heat pipe thermocouples locations are presented in Fig. 3.

3. Numerical model

3.1. Model geometry and computational mesh

To investigate the CFD modelling of the three-leg heat pipe, 2D simulations were carried out in ANSYS fluent. The work by Fadhl [39,40] reveals that the behaviour of the two-phase model is the same for both 2D and 3D geometries which encourages the selection of a 2D geometry to make the simulation simpler. The simulations were chosen to be 2D to reduce the calculation time.

To select a suitable mesh, a mesh sensitivity analysis was conducted. Indeed, the simulation results can vary significantly depending on the quality of the mesh. In this regard, five mesh have been implemented and compared: Very coarse, Coarse, Medium, Fine, and Very fine. For each mesh, the size of the hexahedron elements was decreased from 0.7 mm to 0.4 mm. Near the wall, inflation layers were used to capture the near wall phenomena. Depending on the size of the mesh, the number of inflation layer was increased to improve the simulation accuracy. The mesh metrics of all the compared mesh were checked in terms of skewness, aspect ratio, average orthogonal quality, and average element quality. The 2D geometry used for the simulation and the five compared mesh are presented in Fig. 4.

To conduct the mesh sensitivity analysis, 20s of heat pipe operation was simulated. The Lee [8] model source terms were implemented using a C-code UDF. The saturation temperature was set to

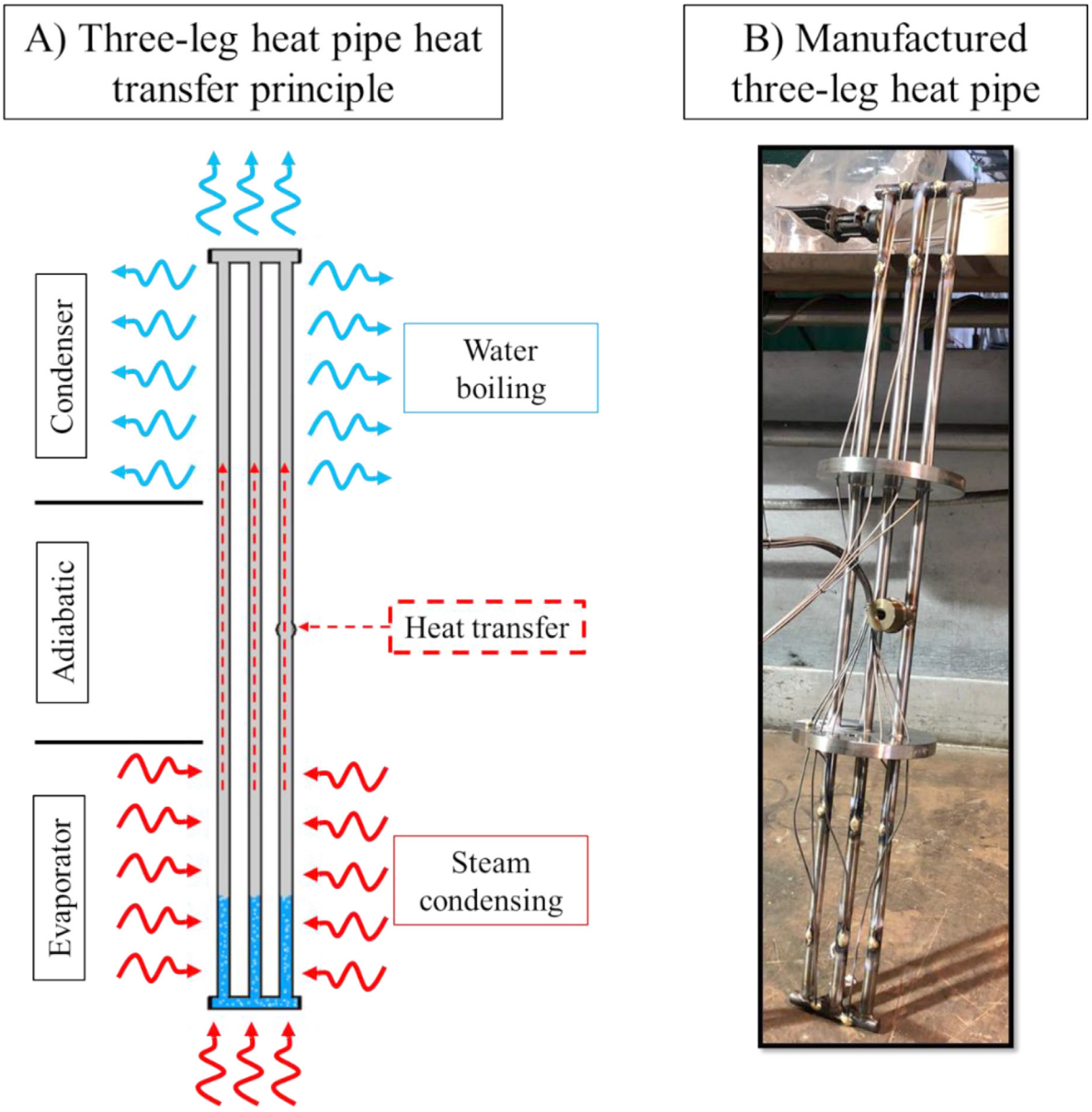

Fig. 1. Three-leg heat pipe prototype and heat transfer principle.

290 K, and the mass transfer coefficients were kept to their default values of 0.1 s^{-1}. For both evaporator and condenser, constant heat flux of 764.5 W/m^2 were imposed on the walls. R134a was used as a working fluid with temperature dependent properties extracted from NIST database [41]. The simulations were initialised at a temperature of 290 K with a saturation pressure for R134a of 518150 Pa. In Fig. 5 are presented the results from the mesh sensitivity analysis.

On top of Fig. 5 are presented the simulated heat pipe temperature for the different tested mesh. With an increase of the number of elements in the mesh, the heat pipe temperature converges to a given value. To guarantee an accuracy of the result, the selected mesh must converge to temperatures close to that of the finer mesh tested. If the Very Coarse mesh result are surprisingly accurate, the Coarse and Medium mesh result converge to values up to 0.14 K away from the Very Fine mesh. This is shown at the bottom of Fig. 5 where the difference of temperature with the finer mesh is shown. It is observed that, between the Fine mesh and Very Fine mesh, the temperature difference after 20 s is lower than 0.02 K. Yet, when selecting a mesh, the accuracy of the simulation's results must be balance with the calculation time. In particular, for transient two-phase simulation, the calculation time can be very important and represents a real challenge. For instance, the calculation time for the mesh sensitivity analysis is shown in Fig. 5. It is observed that an increase of the number of elements in the mesh greatly increases the calculation time. For the Very Coarse and Coarse mesh, the calculation time remained reasonable and lower than 10 days. However, for the Fine and Very Fine mesh, it took respectively more than 25 days and 87 days to simulate 20 s of heat pipe simulation. As such, to balance the simulation accuracy and calculation time, the Fine mesh was selected for the three-leg heat pipe simulation.

3.2. Multi-phase model and source terms

For the simulation of the three-leg heat pipe, the Euler-Euler Volume of Fluid (VOF) approach with the Lee [8] model was used as this model was widely recommended in the literature [16–28].

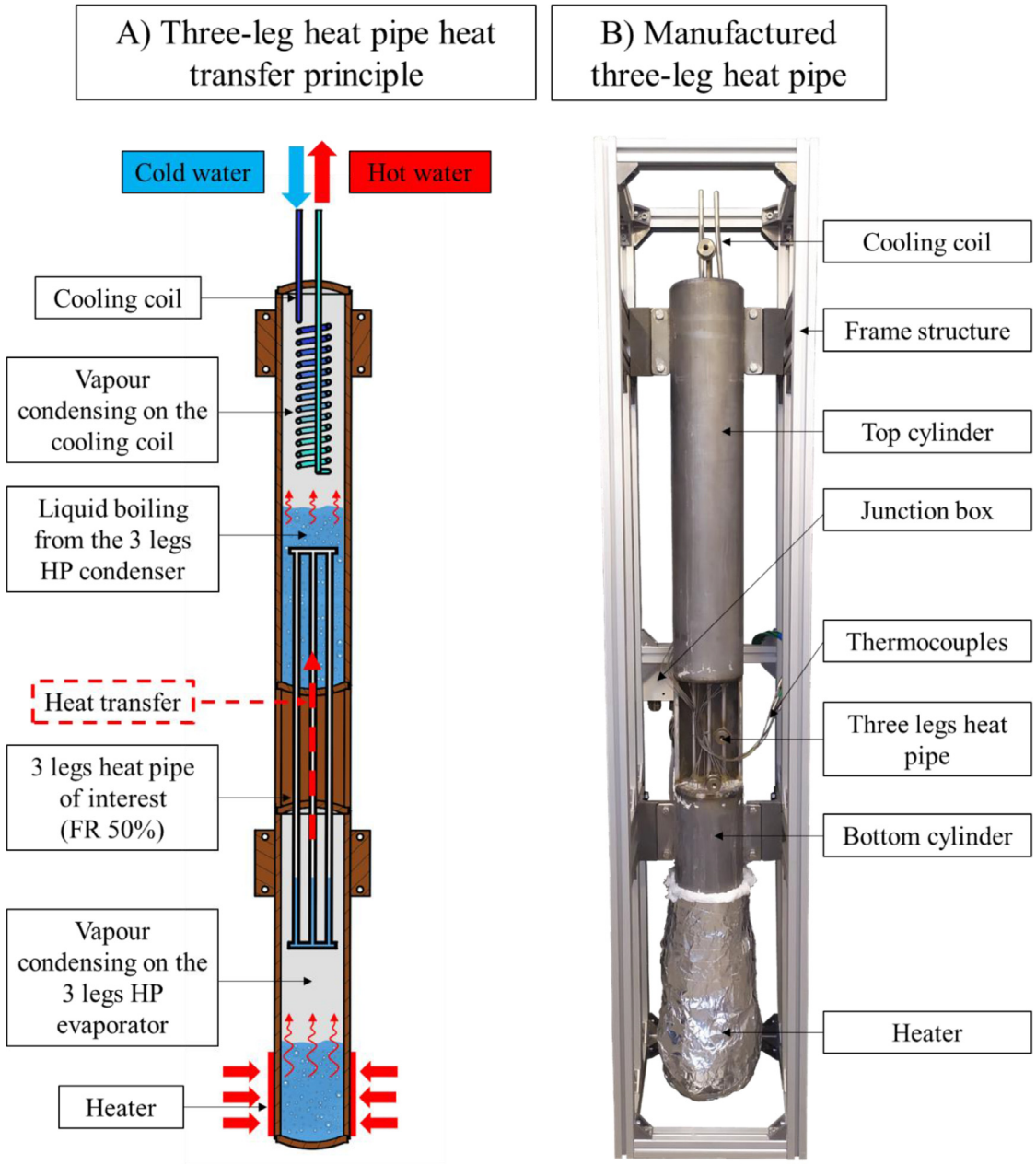

Fig. 2. Three-leg heat pipe assembly and complete heat transfer principle.

The Lee [8] model source terms are given by [42–44]: where $S_{M,l}$ and $S_{M,v}$ are the liquid and vapour phase mass source terms (kg/m^{3}s), β_e and β_c are the evaporation and condensation mass transfer coefficients, α_l and α_v the liquid and vapour phase volume fractions, ρ_l and ρ_v the liquid and vapour densities (kg/m^3), T_{mix} the mixture temperature (K), T_{sat} the saturation temperature (K), and i_{lv} the latent heat of vaporization (J/kg). For both evaporation and condensation, the energy source term S_E is the product of the mass source term with the latent heat: with S_E is the energy source term (J/m^{3}s), S_M the mass source terms (kg/m^{3}s), and i_{lv} the latent heat of vaporization (J/kg).

In the Lee [8] model, three inputs are needed: (1) the saturation temperature T_{sat}, (2) the evaporation mass transfer source term β_e, and (3) the condensation mass transfer source term β_c. If the value of the saturation temperature is always chosen by the user, the evaporation and condensation mass transfer coefficients are often kept to their default values of 0.1 s^{-1}. Yet, in the literature, other values of mass transfer coefficient were tested. In the conducted simulation of the three-leg heat pipe, different values of saturation temperature T_{sat} were used and compared. To study the impact of the saturation temperature of the simulation results, the saturation temperature was set to 290 K and 300 K. The impact of the mass transfer coefficient on the result was investigated using the study from Kim et al. [22]. As the included Lee [8] model of ANSYS has been reported as uncapable to simulate two-phase heat transfer, three types of Lee models were investigated and compared: (1) the included Lee model, (2) the usual user defined functions (UDF) Lee model, (3) a modified UDF Lee model. The modified UDF Lee model includes an additional user defined function which aims at directly obtaining the value of the saturation temperature from the simulation. The UDFs were developed using C-code and compiled to ANSYS Fluent (Tables 1 and 2).

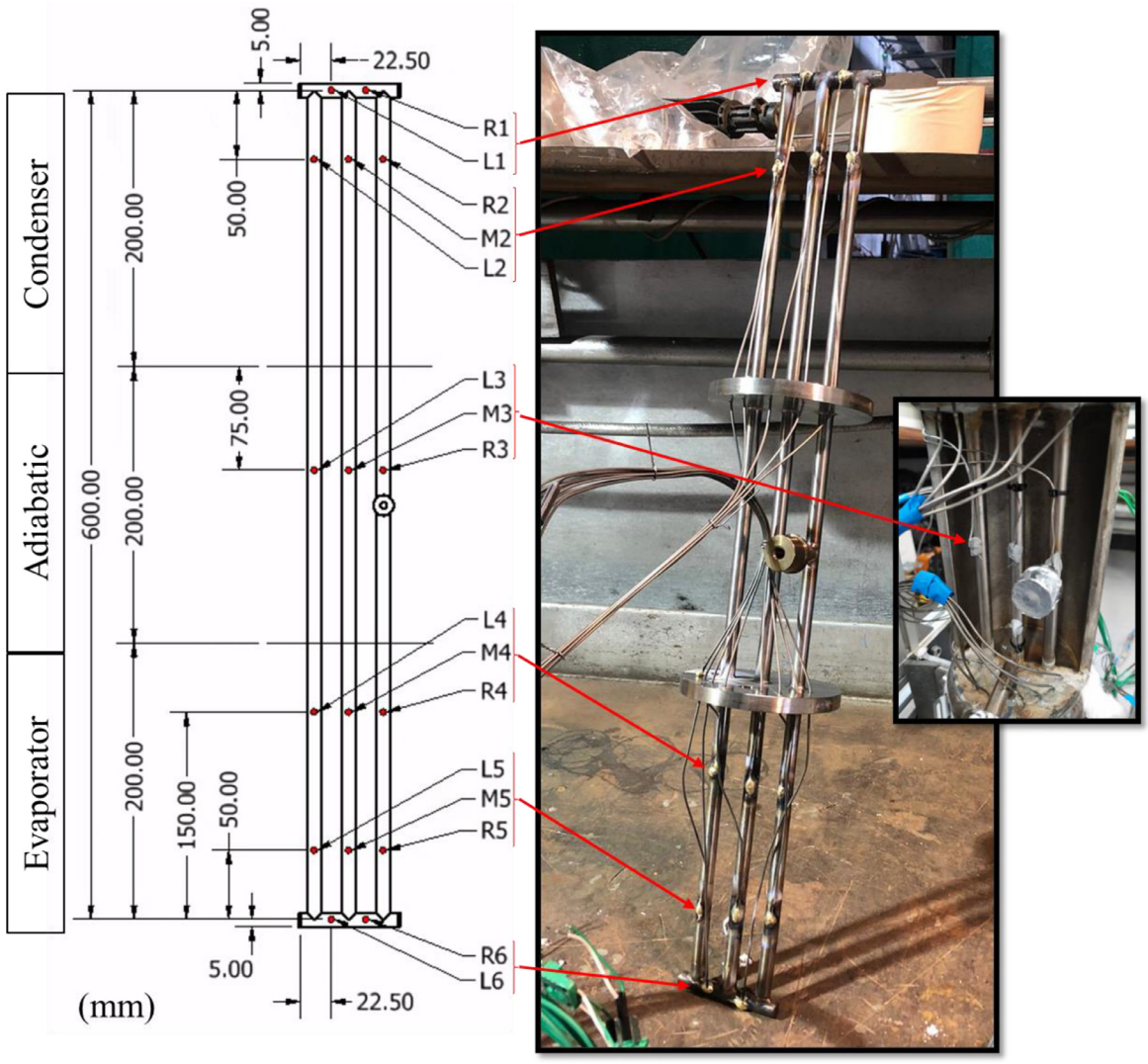

Fig. 3. Three-leg heat pipe and thermocouple's location.

Table 1
Lee [8] model mass source terms.

Process	Condition	Mass source term
Evaporation	$T_{mix} > T_{sat}$	$S_{M,l} = -S_{M,v} = -\beta_e \alpha_l \rho_l \frac{T_{mix} - T_{sat}}{T_{sat}}$
Condensation	$T_{sat} < T_{mix}$	$S_{M,l} = -S_{M,v} = \beta_c \alpha_v \rho_v \frac{T_{sat} - T_{mix}}{T_{sat}}$

Table 2
Lee [8] model energy source terms.

Process	Condition	Energy source term
Evaporation	$T_{mix} > T_{sat}$	$S_E = i_{lv} S_{M,l} = -i_{lv} S_{M,v} = -\beta_e \alpha_l \rho_l i_{lv} \frac{T_{mix} - T_{sat}}{T_{sat}}$
Condensation	$T_{sat} < T_{mix}$	$S_E = i_{lv} S_{M,l} = -i_{lv} S_{M,v} = \beta_c \alpha_v \rho_v i_{lv} \frac{T_{sat} - T_{mix}}{T_{sat}}$

3.3. Boundary and initial conditions

In the conducted simulation, a heat transfer rate of 1000 W was aimed. This was selected to generate high temperature gradients through the three-leg heat pipe and ease the observation of the two-phase cycle. As such, based on the evaporator's wall area, a constant heat flux of 764.5 W/m^2 was imposed on the evaporator's wall. At the condenser's wall, two boundary conditions were implemented and compared. Indeed, in the literature, both constant heat flux and convective heat transfer coefficient were implemented as boundary conditions for the heat pipe condenser. When a constant heat flux boundary condition was imposed, a heat flux of -764.5 W/m^2 was set. When a forced convective heat transfer coefficient boundary condition was selected, a heat transfer coefficient $h_{convection}$=140 W/m^{2}K was imposed with a free stream temperature of 290 K which was estimated by considering pool boiling heat transfer in the top cylinder with the Rohsenow [45] correlation. This heat transfer coefficient was calculated based on the pool boiling heat transfer coefficient taking place outside of the three-leg heat pipe condenser's wall. The heat pipe temperature was initialized at 290 K for the complete thermosyphon geometry. The pressure was initialised at 518,149 Pa which is the saturation pressure of R134a at 290 K.

3.4. Solution procedure

In this study, transient simulations were carried out. The time step was adjusted to maintain a stable simulation but was never increased above 0.0001 s. Gravity was enabled. In this work, the influence of the turbulence model was not studied. Based on the reference work from Fadhl [30,40] who used a laminar turbulence model and found it suitable for the simulation of thermosyphons, the laminar turbulence model was selected. The SIMPLE algorithm was combined with first-order upwind schemes for the momen-

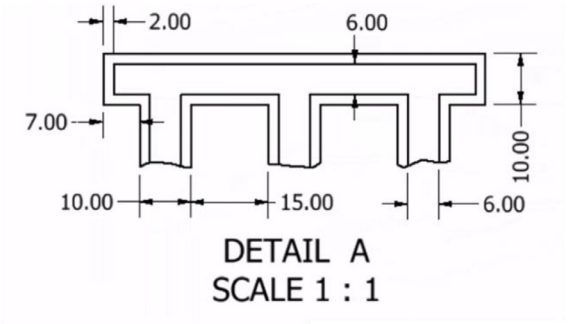

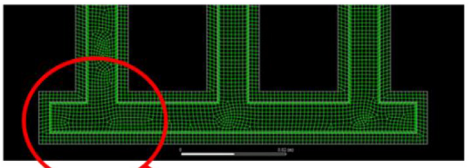

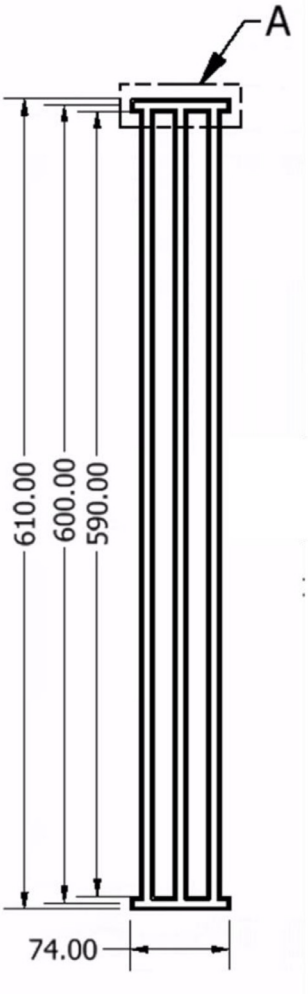

Mesh	Elements	Element's size (mm)	Inflation layers	Overview
Very coarse	52331	0.7	3	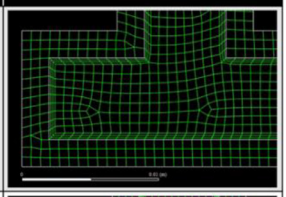
Coarse	108056	0.5	5	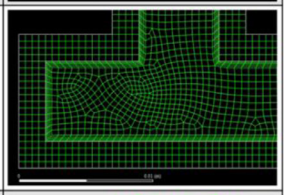
Medium	145528	0.5	10	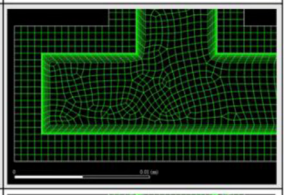
Fine	203304	0.4	10	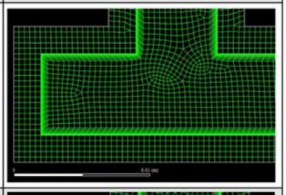
Very fine	252805	0.4	15	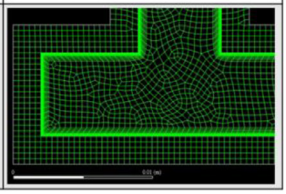

Fig. 4. 2D geometry of the three-leg heat pipe simulations and compared mesh.

tum and energy transport equations. For the phase volume fraction and pressure interpolation scheme, Geo-reconstruct and PRESTO discretization were used.

4. Theoretical model

For the theoretical modelling of the three-leg heat pipe, a thermal resistance network was used and considered the influence of the multi-channel geometry. To further validate the recently proposed model, the thermal resistance network reported in the work by Guichet et al. [38] was used to predict the performance of the three-leg heat pipe. This thermal resistance network considers different thermal resistances for each parallel channel, bottom collector, and top collector. This multi-channel heat pipe thermal resistance network can be adapted to predict the thermal performance of a heat pipe with any number of parallel channels. The multi-channel thermal resistance network is presented in Fig. 6.

In the above thermal resistance network, $R_{ext,}$ is the external thermal resistance taking place at the outer wall of the evaporator and condenser, $R_{wall,ax}$ is the axial conduction thermal resistance. The axial conduction thermal resistance of the three-leg heat pipe is given by [46]:

$$R_{wall,ax} = \frac{(L_a + 0.5L_c + 0.5L_e)}{k_{alum}A_{cs}} \quad (1)$$

where L_e, L_a, L_c are the evaporator, adiabatic, and condenser length respectively (m), and A_{cs} the cross-section area of the heat pipe which is filled by solid material. In the multi-channel thermal resistance network proposed, several radial conduction thermal resistances are included: $R_{wall,e\ channel}$ is the conduction thermal

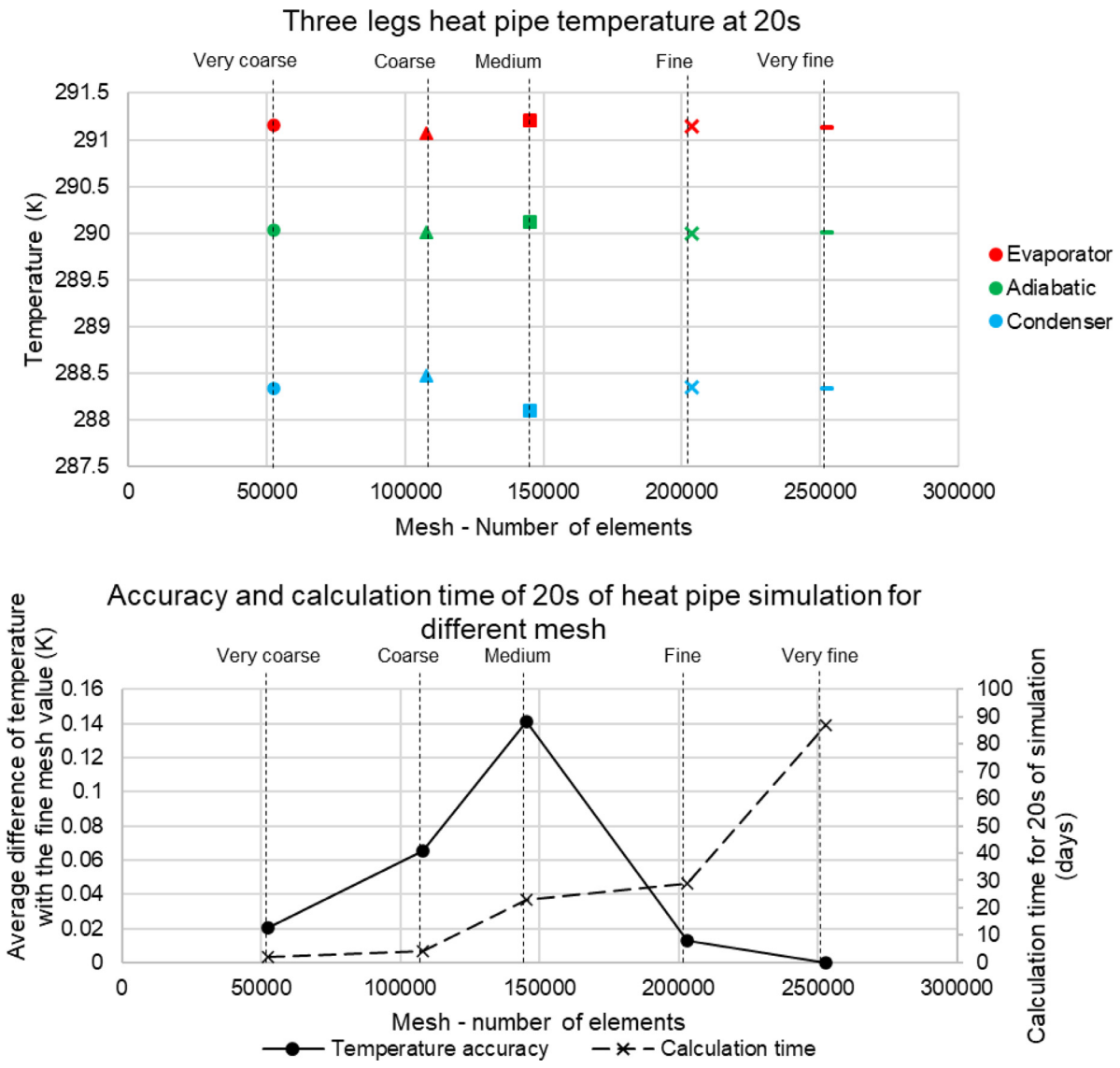

Fig. 5. Mesh sensitivity analysis results.

resistance of a single channel at the evaporator, $R_{wall,e\ bottom\ collector}$ is the conduction thermal resistance of the bottom collector at the evaporator, $R_{wall,c\ channel}$ is the conduction thermal resistance from a single channel at the condenser, and $R_{wall,c\ top\ collector}$ is the conduction thermal resistance from the top collector at the condenser. The radial conduction thermal resistances were calculated using [47]:

$$R_{wall,e-1\ channel} = \frac{\ln\left(D_{o,1\ channel}/D_{i,\ 1\ channel}\right)}{2\pi k_w L_{e,\ 1\ channel}} \quad (2)$$

with $D_{o,\ 1\ channel}$ the outer diameter of the channel tube (m), $D_{i,1\ channel}$ the inner diameter of the channel tube (m), k_w the wall thermal conductivity (W/m.K), and $L_{e,\ 1\ channel}$ the evaporator length of the channel (m). To estimate the pool boiling, falling film boiling, and condensation thermal resistances of the parallel legs and collectors, correlations had to be used to estimate the corresponding heat transfer coefficient h:

$$R = 1/Ah \quad (3)$$

with A the heat transfer area (m^2). To identify the most suitable heat transfer coefficient correlations, the available correlations from the literature were compared to the local heat transfer coefficient measured experimentally. For the pool boiling heat transfer coefficient in the bottom collector, the correlation from Shiraishi et al. [48] was used:

$$h_{pb,\ Shiraishi} = 0.32\left(\frac{\rho_l^{0.65} k_l^{0.3} c_{p,l}^{0.7} g^{0.2}}{\rho_v^{0.25} i_{lv}^{0.4} \mu_l^{0.1}}\right)\left(\frac{P_v}{P_{atm}}\right)^{0.23} q''^{0.4}_{pb} \quad (4)$$

where $h_{pb,\ Shiraishi}$ is the pool boiling heat transfer coefficient predicted by the correlation from Shiraishi et al. [48] (W/m^2K), $A_{pb,e-bottom\ collector}$ is the pool boiling area in the bottom collector (m^2), ρ_l and ρ_v the liquid and vapour densities (kg/m^3), k_l the liquid thermal conductivity (W/m.K), $c_{p,l}$ the specific heat (J/kg.K), g the gravitational acceleration (m/s^2), i_{lv} the latent heat of vaporization (J/kg), μ_l the liquid dynamic viscosity (Pa.s), P_v the saturated vapour pressure (Pa), P_{atm} the atmospheric pressure (Pa), and q''_{nb} the pool boiling heat flux (W/m^2). The pool boiling heat transfer coefficient in the legs was predicted using the Imura et al. [49] correlation:

$$h_{pb,\ Imura} = 0.32\left(\frac{\rho_l^{0.65} k_l^{0.3} c_{p,l}^{0.7} g^{0.2}}{\rho_v^{0.25} i_{lv}^{0.4} \mu_l^{0.1}}\right)\left(\frac{P_v}{P_{atm}}\right)^{0.3} q''^{0.4}_{pb} \quad (5)$$

Unexpectedly, in the three-leg heat pipe prototype, falling film boiling did not occur. The thermocouples at the top of the evapora-

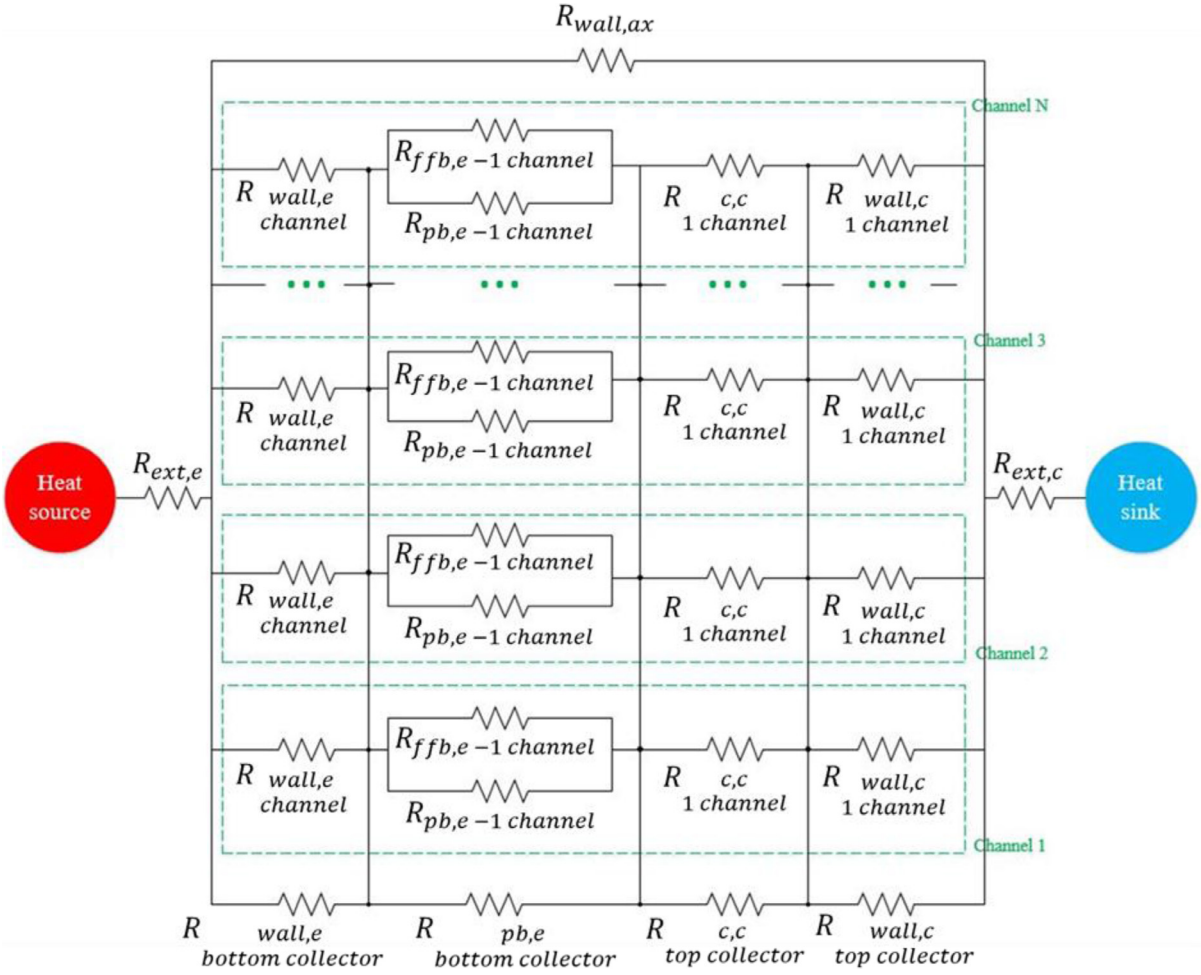

Fig. 6. Multi-channel flat heat pipe thermal resistance model.

tor revealed that pool boiling heat transfer took place in the whole volume of the evaporator. This was assumed to be due to an inaccurate charge of the heat pipe as the amount of liquid introduced is very small. For the condensation heat transfer coefficient, the same correlation was used for the top collector and for the parallel legs. It was found that the most suitable correlation was the correlation from Schnabel and Palen [50]:

$$h_c = \frac{0.0283(Re_f/4)^{7/24}Pr_l^{1/3}}{1+9.66(Re_f/4)^{-3/8}Pr_l^{-1/6}}k_l\left(\frac{\mu_l^2}{\rho_l(\rho_l-\rho_v)g}\right)^{-1/3} \quad (6)$$

where,

$$Re_{f,L_c} = \frac{4\Gamma_{L_c}}{\mu_l}$$

with Re_f the falling film Reynolds number, Γ_{L_c} the mass flow rate of liquid per unit periphery (kg/m.s), μ_l the liquid dynamic viscosity (Pa.s), ρ_l and ρ_v the liquid and vapour densities (kg/m^3), and g the gravitational acceleration (m/s^2). To calculate the pool boiling and condensation heat transfer coefficients, the wall temperatures and vapour temperatures are needed. However, such temperatures are unavailable as these can only be obtained by first estimating the thermal resistances. In this regard, an iterative tool was built which first assumes the wall temperature and corrects it after consecutive iterations. To prevent the transmission of errors in the theoretical model, the bottom cylinder and top cylinder thermal resistances were not predicted theoretically. The iterative tool integrated the described multi-channel heat pipe thermal resistance model and runs iterations until an energy balance is reached between the heat pipe temperature and heat transfer rate. More details about the theoretical model can be found in the work by Guichet et al. [38].

5. Data reduction

To analyse the experimental data from the three-leg heat pipe, data reduction equations were used. The heat transfer rate passing through the system was calculated using the Newton's law of cooling:

$$\dot{Q} = \dot{m}_{water}c_{p,water}(T_{water,\ out} - T_{water,\ in}) \quad (7)$$

where $\dot{Q}$ is the heat transfer rate through the system (W), $\dot{m}_{water}$ is the water flow rate in the cooling manifold (kg/s), $c_{p,water}$ is the specific heat of water (J/kg.K), and $T_{water,\ out}$ and $T_{water,\ in}$ are the water temperature at the outlet and inlet (K), respectively. To characterise the three-leg heat pipe thermal performance, several thermal resistances were calculated. The boiling, condensation and total thermal resistances of the three-leg heat pipe were calculated from:

$$R_{boiling} = \frac{(T_{evaporator} - T_{adiabatic})}{\dot{Q}} \quad (8)$$

$$R_{condensation} = \frac{(T_{adiabatic} - T_{condenser})}{\dot{Q}} \quad (9)$$

$$R_{HP} = \frac{(T_{evaporator} - T_{condenser})}{\dot{Q}} \quad (10)$$

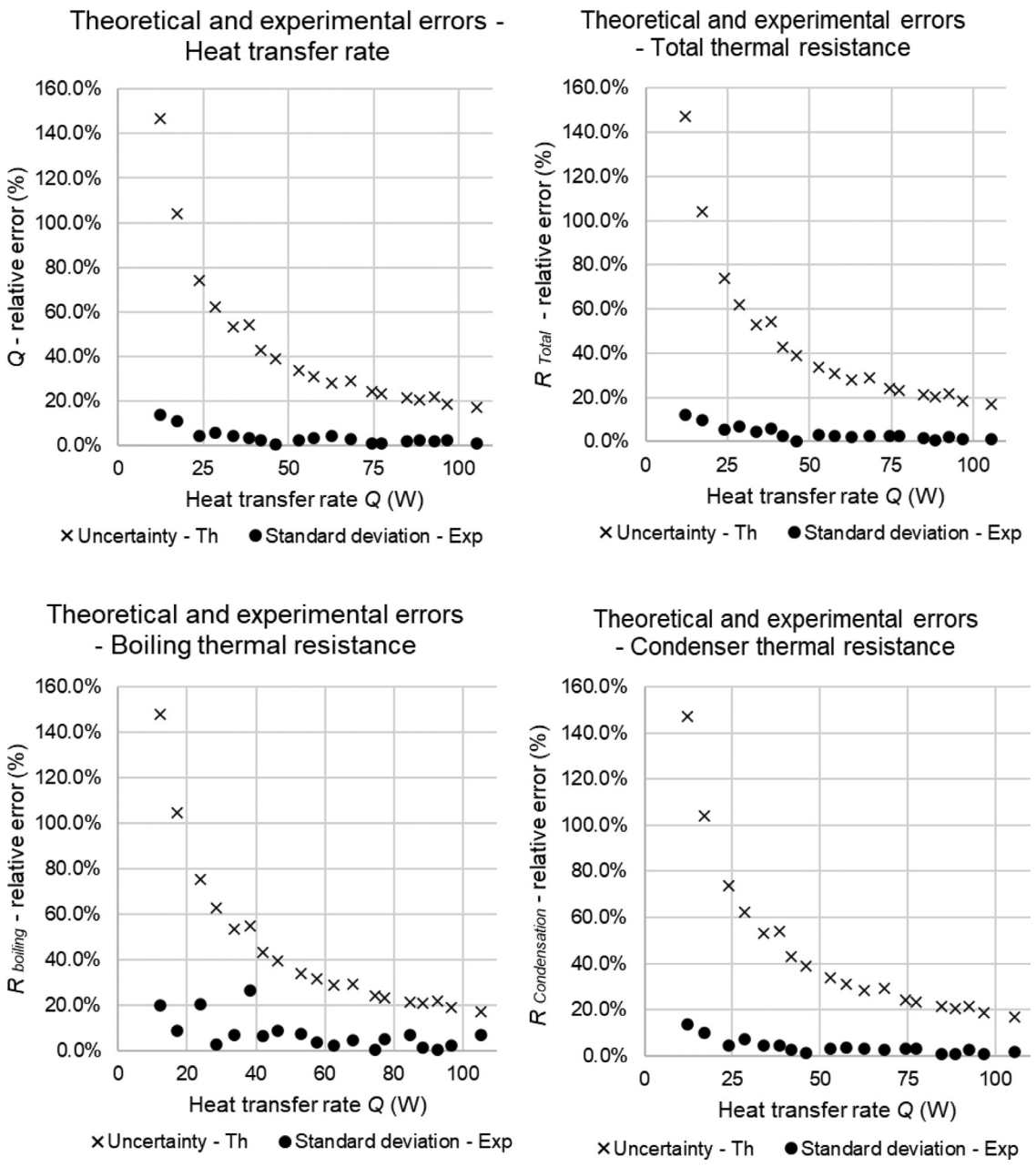

Fig. 7. Theoretical and experimental errors of the measured heat transfer rate and total, boiling, and condensation thermal resistances during the three-leg heat pipe experiments.

where $R_{boiling}$, $R_{condensation}$, and R_{HP} are the boiling, condensation, and total heat pipe thermal resistances (K/W), $T_{evaporator}$, $T_{adiabatic}$, and $T_{condenser}$ the evaporator, adiabatic, and condenser temperatures (K), and $\dot{Q}$ the heat transfer rate (W). The respective experimental heat transfer coefficients were measured using:

$$h = \frac{1}{AR} \tag{11}$$

with h the heat transfer coefficient (W/m²K), A the heat transfer area (m²), and R the thermal resistance (K/W).

6. Error propagation and standard deviation

In the objective of estimating the experimental error made during the testing of the three-leg heat pipe, the error propagation was studied. This approach aims at estimating the uncertainties from the experimental sensors and the errors conveyed to the calculated values of heat transfer rate, thermal resistances, and heat transfer coefficients. During the three-leg heat pipe testing, two types of measurement occurred. The cooling water mass flow rate was measured by sampling a given volume of water for 10s. Temperature measurements were taken from K-type thermocouples which inaccuracy was estimated by comparing their measurements while immersed in boiling water. The estimated measurement uncertainties for the three-leg heat pipe experiments are reported in Table 3 below.

From the estimated measurements uncertainties, the error made on the estimation of the heat transfer rate $S_{\dot{Q}}$ was estimated using:

$$S_{\dot{Q}} = \dot{Q}\sqrt{\left(\frac{S_{\dot{m}_{water}}}{\dot{m}_{water}}\right)^2 + \left(\frac{S_{\Delta T_{water}}}{\Delta T_{water}}\right)^2} \tag{12}$$

Table 3
Estimated measurement uncertainties.

Flow rate manual measurement	$S_{V_{water\ in\ 10s,\ manual}}$	2.5 ml
Thermocouple	S_T	0.2 K

with $\dot{Q}$ the heat transfer rate (W), $S_{\dot{m}_{water}}$ the uncertainty related to the water mass flow rate $\dot{m}_{water}$ (kg/s), $S_{\Delta T_{water}}$ the uncertainty related to the difference of cooling water temperature (K), and ΔT_{water} the temperature difference between the outlet and inlet of the cooling water (K). To estimate the error propagated to the boiling, condensation, and total thermal resistances of the three-leg heat pipe, the following equations are used:

$$S_{R_{boiling}} = R_{boiling}\sqrt{\frac{S_{T_{evaporator}}^2 + S_{T_{adiabatic}}^2}{(T_{evaporator} - T_{adiabatic})^2} + \left(\frac{S_{\dot{Q}}}{\dot{Q}}\right)^2} \quad (13)$$

$$S_{R_{condensation}} = R_{condensation}\sqrt{\frac{S_{T_{adiabatic}}^2 + S_{T_{condenser}}^2}{(T_{adiabatic} - T_{condenser})^2} + \left(\frac{S_{\dot{Q}}}{\dot{Q}}\right)^2} \quad (14)$$

$$S_{R_{HP}} = R_{HP}\sqrt{\frac{S_{T_{evaporator,pb}}^2 + S_{T_{condenser}}^2}{(T_{evaporator,pb} - T_{condenser})^2} + \left(\frac{S_{\dot{Q}}}{\dot{Q}}\right)^2} \quad (15)$$

In the above, $R_{boiling}$, $R_{condensation}$, and R_{HP} are the boiling, condensation, and total heat pipe thermal resistances (K/W), $T_{evaporator}$, $T_{adiabatic}$, and $T_{condenser}$ the evaporator, adiabatic, and condenser temperatures (K), and $\dot{Q}$ the heat transfer rate (W) and S_x the corresponding uncertainty of the variable x.

Based on the error propagation equations, the experimental error was estimated theoretically. This theoretical uncertainty was also compared to the standard deviation between similar experiments. Indeed, to improve the accuracy of the results, each experiment was repeated at least five times. The theoretical uncertainties and experimental standard deviation for the calculated heat transfer rate, total thermal resistance, boiling thermal resistance, and condensation thermal resistance of the three-leg heat pipe are presented in Fig. 7.

From Fig. 7 is observed that, due to the low heat transfer rates investigated, the estimated uncertainty of the heat transfer rate is relatively high. Based on the error propagation method, a theoretical error of 140% is expected while estimating a heat transfer rate around 10W. This can be explained as the low heat transfer rates tested implied a low difference of temperature between the cooling water inlet and outlet. As such, the thermocouples uncertainty becomes significant. With an increase of the heat transfer rate, the temperature difference between the inlet and outlet increases and, as a result, the uncertainty decreases significantly. Consequently, the heat transfer rate uncertainty drops to 40% at 50 W and to 20% at 100 W. The high uncertainty in the estimation of the heat transfer rate has a direct impact on the theoretical uncertainty of the three-leg heat pipe thermal resistances. Indeed, to calculate the three-leg heat pipe thermal resistances, the heat transfer rate is needed. From Fig. 7, it can be seen that the theoretical uncertainties for the total, boiling, and condensation thermal resistances are similar to that of the heat transfer rate. Again, the theoretical uncertainties decrease significantly with an increase of the heat transfer rate because the difference of temperature between the cooling water inlet and outlet increases. Those theoretical uncertainties highlight the difficulty of accurately measuring the heat transfer rate. In this regard, to improve the accuracy of the results, each experiment was repeated five times minimum. The measured standard deviation between similar experiments revealed a satisfactory reproducibility. Indeed, even at very low heat transfer rates (~10 W), the standard deviation between similar experiments is lower than 20%.

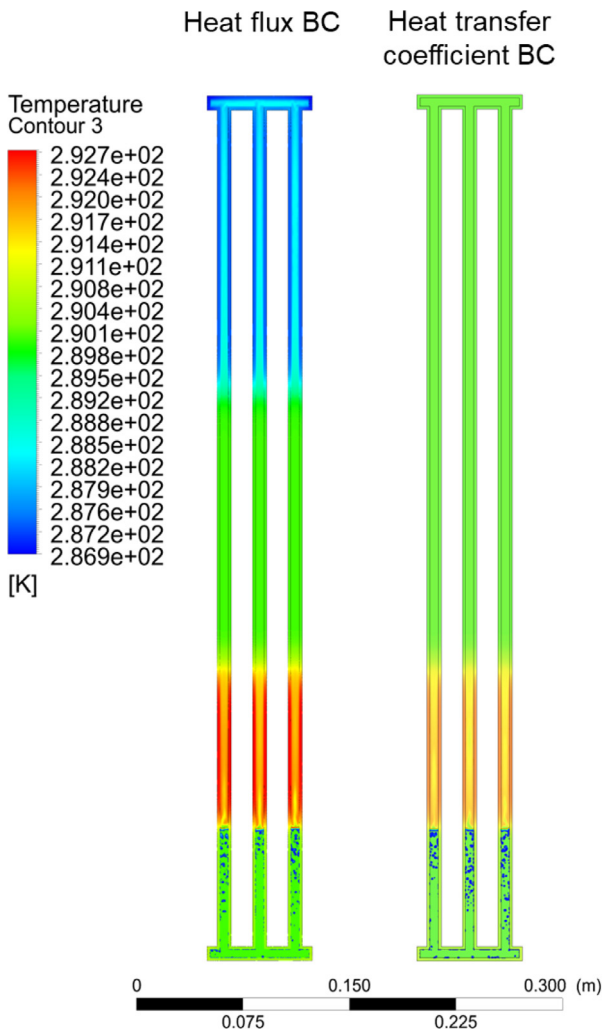

Fig. 8. Boundary condition comparison.

7. Results

7.1. Numerical model results

In this section, the numerical (CFD) modelling of the three-leg heat pipe is studied.

7.1.1. Boundary condition comparison

In the numerical simulation of heat pipes, both constant heat flux and convection heat transfer coefficient boundary conditions have been imposed on the wall of the condenser. As such, both boundary conditions have been compared. For this comparison, the evaporator's heat flux was maintained at 764.5 W/m^{2}K and the heat pipe temperature was initialized at 290 K. The saturation temperature was also set to 290 K. In Fig. 8 are shown the temperature and volume of fluid contours of the three-leg heat pipe after 20 s for both condenser's boundary condition.

From Fig. 8, it is observed that the temperature profile of the three-leg heat pipe is similar. Vapour bubbles are forming in the liquid pool which remains at the saturation temperature of 290 K. The vapour bubbles are represented in blue by the addition of a Volume-of-Fluid contour which colour does not represent their temperature. In the upper part of the evaporator which is not filled

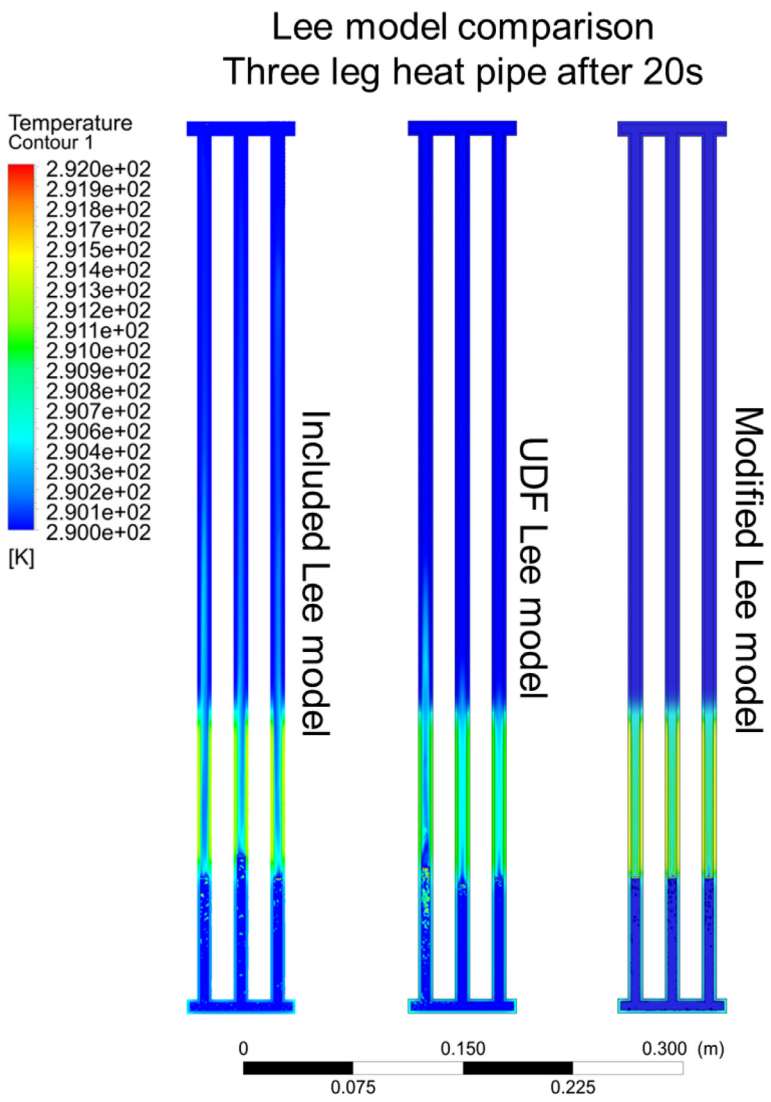

Fig. 9. Lee models' comparison.

with liquid, a zone of higher temperature can be seen. The adiabatic section of the three-leg heat pipe remains at a temperature of 290 K. More interestingly, drastically different temperature profiles of the condenser can be seen. For the heat flux boundary condition, the condenser temperature decreases to 287 K. On the other hand, when a convective heat transfer coefficient is implemented, the condenser temperature tends to converge to values close to the free stream temperature implemented. Physically, the constant heat flux boundary condition has a lower meaning, and the transient temperature profile of the simulated heat pipe may not fit the experimental data. Indeed, a constant heat flux boundary condition always forces the extraction of a fixed heat transfer rate. However, in reality, the heat pipe transiently warms-up and the heat transfer rate delivered to the heat sink is lower than that provided to the evaporator. The heat transfer rate extracted from the heat pipe and recovered by the heat sink is only equal to the input heat transfer rate when steady state is reached. Hence, by forcing the extraction of heat at the beginning of the simulation, the heat pipe temperature at the condenser goes lower than the experiments. In extreme cases, Fig. 8 even shows that a constant heat flux boundary condition at the condenser can force the heat pipe temperature to decrease to values lower than the initial temperature. Hence, a constant heat flux boundary condition is considered less accurate and does not allow the visualisation of the increase of heat pipe temperature. On the other hand, a convection heat transfer coefficient is more suitable to observe the temperature increase of the whole heat pipe. Finally, the transient temperature profile is expected to be more accurate as the heat transfer rate at the condenser will be lower than that given at the evaporator until steady state is reached. In this regard, a convection heat transfer coefficient boundary condition is advised for the simulation of heat pipes. For the following simulations of the three-leg heat pipe, this boundary condition was implemented on the condenser's wall.

7.1.2. Lee model comparison

In the literature, the Lee [8] model has been largely preferred for the simulation of heat pipes [16–28]. However, up to today, the included Lee [8] model of ANSYS was described as unable to simulate heat pipes and that the use of user defined functions (UDFs) was required [9,17,20,21,27,30,40,51]. However, with the new updates of ANSYS, the included Lee [8] model was modified. In this regard, for the simulation of the three-leg heat pipe, both included Lee [8] model and UDF Lee [8] model were implemented and compared. For both Lee [8] models, the initial heat pipe temperature and the saturation temperature were set to 290 K.The mass transfer coefficients were kept at their default values of 0.1 s^{-1}. A modified UDF Lee [8] model was also developed and tested. This Lee

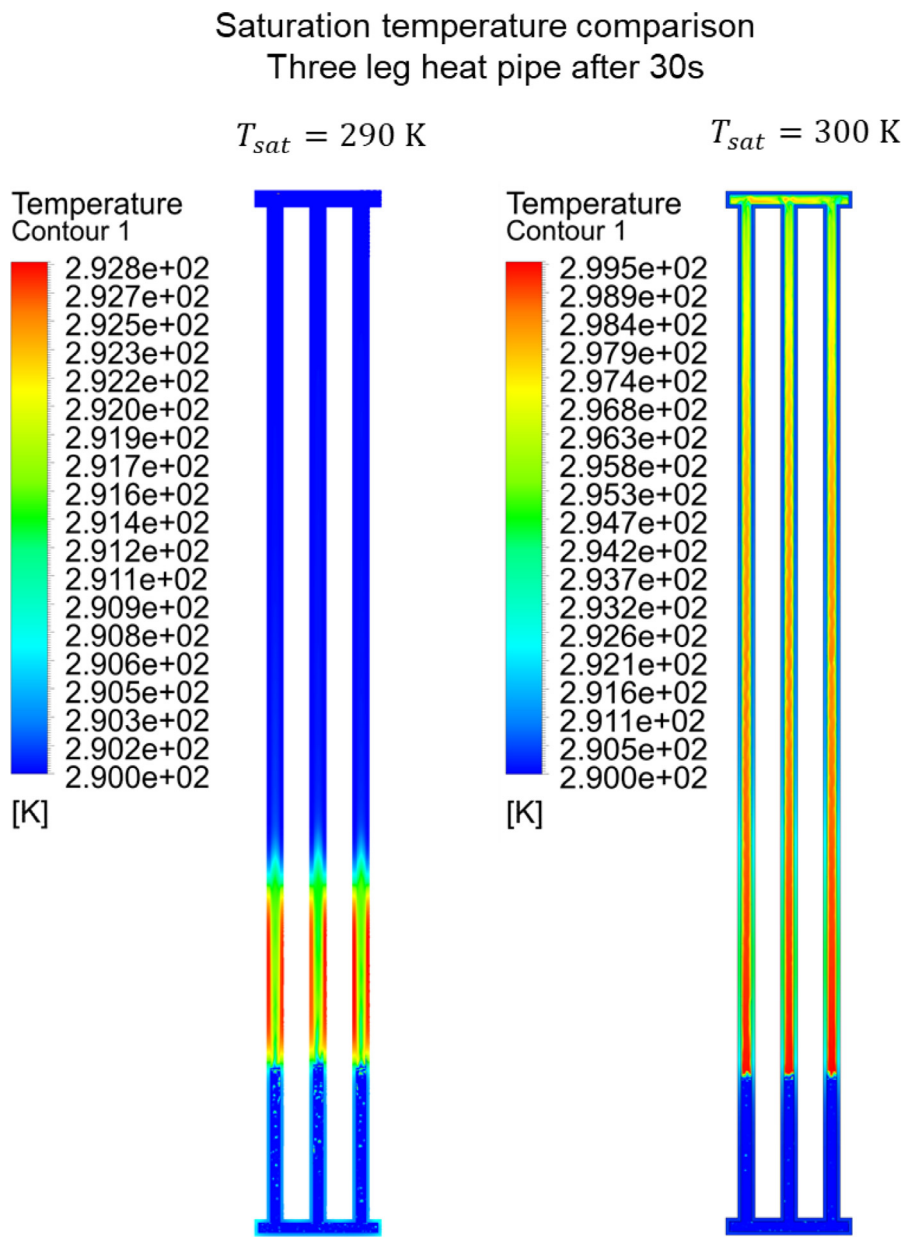

Fig. 10. Impact of the saturation temperature input.

[8] model aimed at modifying the saturation temperature value based on the temperature of the liquid pool. To do so, a UDF was codded to measure the temperature of the liquid pool. This temperature was then fed to the Lee [8] model and used as the new saturation temperature. In Fig. 9 are shown the temperature and volume of fluid contours of the three compared Lee [8] models after 20 s of three-leg heat pipe simulation.

From Fig. 9 can be observed that the difference between the three Lee [8] models is small. For both Included Lee [8] model and UDF Lee [8] model, vapour bubbles are observed in the liquid pool. The boiling activity is more important near the surface which makes the liquid level fluctuate. After 20 s, the temperature of the liquid pool remains at a saturation temperature of 290 K. In the evaporator's volume which is filled by vapour, a temperature increase is observed. This temperature increase is created due to the absence of liquid film on the wall. Indeed, the amount of condensed falling film simulated from the Lee [8] model is small. At the adiabatic section, a slightly higher temperature can be detected in the middle of each channel due to the rising vapour. Yet, the temperature of the vapour volume remains close to the implemented saturation temperature value of 290 K. The Included Lee [8] model showed a good stability and was less computationally demanding than the UDF Lee [8] model simulation. Moreover, in the UDF Lee [8] model, a higher boiling activity was observed in the left leg whereas, for the Included Lee [8] model, all three parallel legs exhibited similar behaviours. Regarding the Modified Lee [8] model proposed, bubbles could be observed in the liquid pool. However, the developed Modified Lee [8] model failed into increasing its value of saturation temperature. Indeed, as the initial temperature of the three-leg heat pipe was set to 290 K, the saturation temperature remained very close to 290 K. In opposition, during the codding of the Modified Lee [8] model, it was expected that both liquid pool temperature and saturation temperature value would increase quickly. Therefore, the proposed Modified Lee [8] model failed into improving the usually used Lee [8] model. Finally, as two-phase heat transfer was observed for the

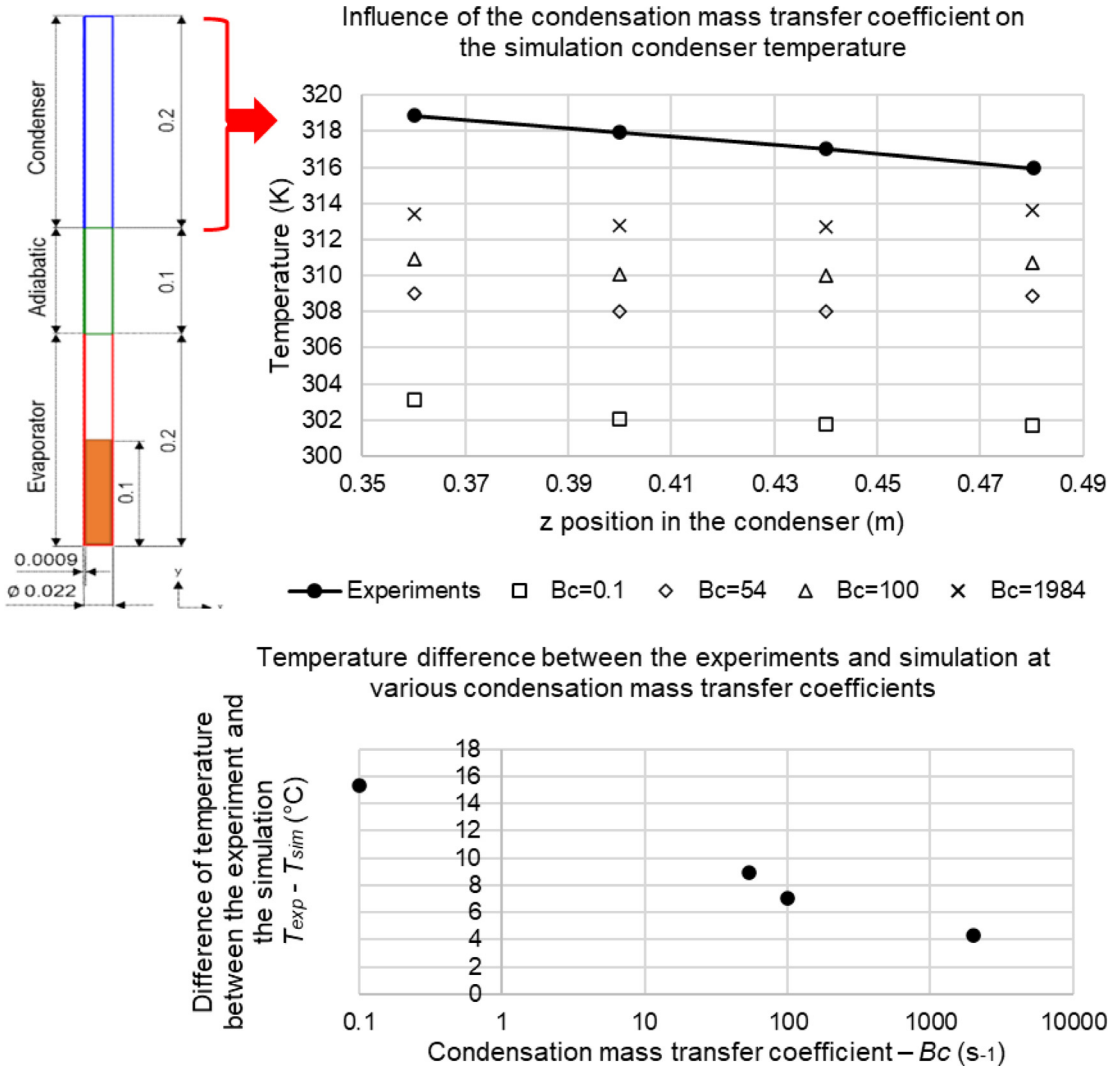

Fig. 11. Impact of the condensation mass transfer coefficient.

included Lee [8] model, that the simulation was relatively stable, and that the computational effort was slightly lower than that of the UDF Lee [8] model, the included Lee [8] model of ANSYS was selected for the simulation of the three-leg heat pipe.

7.1.3. Saturation temperature comparison

The main input required by the Lee [8] model for the simulation of heat pipes is the saturation temperature. This temperature is used as a criterion for the occurrence of boiling and condensation. If the temperature of a cell is higher than the saturation temperature, boiling occurs. On the opposite, if the temperature of a cell is lower than the saturation temperature, condensation takes place. A main limit in the Lee [8] model is the incapacity of estimating the saturation temperature using the CFD software. As a result, up to today, researchers have used experimental data such as the temperature of the heat pipe adiabatic section to be used as the saturation temperature input of the Lee [8] model. However, as demonstrated in Fig. 10, the saturation temperature input has a major impact on the simulation results.

In Fig. 10, two values of saturation temperature are compared: 290 K and 300 K. The temperature and volume of fluid contours of the three-leg heat pipe after 30s are shown. It can be immediately noted that the temperature profile of the three-leg heat pipe is significantly different for both implemented saturation temperature inputs. In the case where the saturation temperature input was 290 K, the adiabatic and condenser section's temperature remains at 290 K. At the evaporator, a maximum temperature increase of 2 °C is observed in the section which is filled with vapour. Hence, it seems that, when the saturation temperature is similar to the initial temperature, two-phase heat transfer is not triggered, and the heat pipe temperature does not increase. However, in the case where the saturation temperature input is set to 300 K, a clear increase of temperature inside the three-leg heat pipe is observed. In this case, heat transfer takes place from the bottom of the three-leg heat pipe to the top. According to the conducted simulation, the vapour temperature seems to converge to the saturation temperature given. Indeed, when the saturation temperature was set to 300 K, the vapour temperature increases to values close to 300 K. This represents an important limit of the Lee [8] model which seems to force the simulation to converge to temperatures close to the saturation temperature input. Another factor which can be noted from Fig. 10 is that the temperature of the liquid pool remains at an initial temperature of 290K. However, in heat pipes, it is not physically possible to have a vapour temperature higher than that of the liquid pool. This highlights the low physical consistency of the Lee [8] model which manages both liquid and vapour phases separately. As a result, the liquid and vapour phases are poorly linked and leads to discrepancies such as that observed in Fig. 10. Finally, one must be aware that the mass transfer coefficients were similar for both simulations but with different implemented satu-

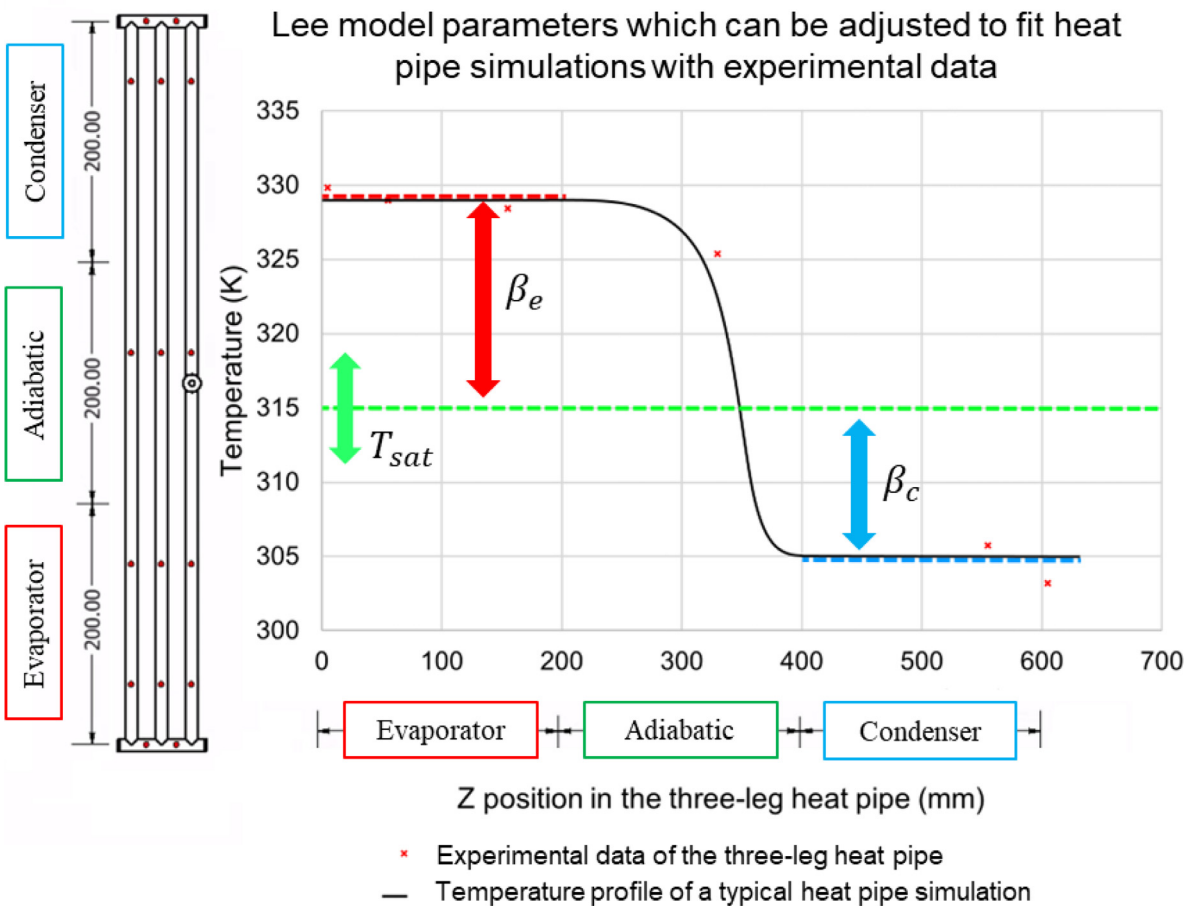

Fig. 12. Lee [8] model inputs that are commonly adjusted to fit heat pipe simulations with experimental data.

ration temperature. Yet, even if the mass transfer rate is similar for both simulations, for the simulation using 290 K as the saturation temperature, the heat transfer is limited. Hence, it seems that, in the Lee [8] model, the mass transfer rate and heat transfer rate are poorly linked. When the Lee [8] model is used, the heat pipe temperature will converge to the implemented saturation temperature value and this regardless of the mass transfer rate.

As a conclusion on the investigation of the impact of the saturation temperature input on the simulation of heat pipes, the following limits of the Lee [8] model were identified:

- The saturation temperature input needed for the Lee [8] model cannot be predicted numerically.
- The vapour temperature converges to the saturation temperature implemented.
- In the Lee [8] model, the liquid and vapour phases are treated separately which can lead to physical nonsense such as a vapour temperature being higher than that of the evaporating liquid pool.
- The link between mass transfer and heat transfer is poor. The mass transfer has little impact on the simulation's temperature.

7.1.4. Mass transfer coefficient comparison

In addition to the saturation temperature, two other inputs are required by the Lee [8] model which are the evaporation mass transfer coefficient β_e and the condensation mass transfer coefficient β_c. In the literature, researchers have usually kept the evaporation mass transfer coefficient at its default value of 0.1 s^{-1}. However, the condensation mass transfer coefficient has been modified by several researchers [19,22,23,28]. In this regard, the impact of the mass transfer coefficient on the simulation of heat pipes must be studied. To do so, the study by Kim et al. [22] is used. In this study, Kim et al. [22] used the Lee [8] model for the simulation of a single thermosyphon and implemented four different values of mass transfer coefficient: 0.1 s^{-1}, 54 s^{-1}, 100 s^{-1}, and 1984 s^{-1}. Those values of mass transfer coefficients were selected by Kim et al. [22] based on suggestions from Refs. [18,19,52,53]. The simulations temperatures were compared to the experimental data from Fadhl et al. [30]. In Fig. 11 are presented the condenser temperatures from the simulation from Kim et al. [22] for various condensation mass transfer coefficients. The simulations' temperatures are compared with the experimental data from Fadhl et al. [30].

From the top graph of Fig. 11 can be observed that, the lower the condensation mass transfer coefficient, the lower the condenser temperature. Indeed, at a mass transfer coefficient of 0.1 s^{-1}, the thermosyphon condenser temperature simulated was close to 302 K whereas, at a mass transfer coefficient of 1984 s^{-1}, the simulated condenser temperature was increased to 313 K. In the bottom graph of Fig. 11 is shown the temperature difference between each simulation and the experimental data. It can be observed that, when the mass transfer coefficient was kept to its default value of 0.1 s^{-1}, the difference of temperature at the condenser between the simulation and the experiments was about 15 °C. When the condensation mass transfer coefficient of the Lee [8] model was increased to 100s^{-1}, this temperature difference decreased significantly to 7 °C. At a condensation mass transfer coefficient of 1984 s^{-1}, the temperature difference between the experiments and the simulation is down to 4 °C. It is therefore concluded that the condensation mass transfer coefficient of the Lee

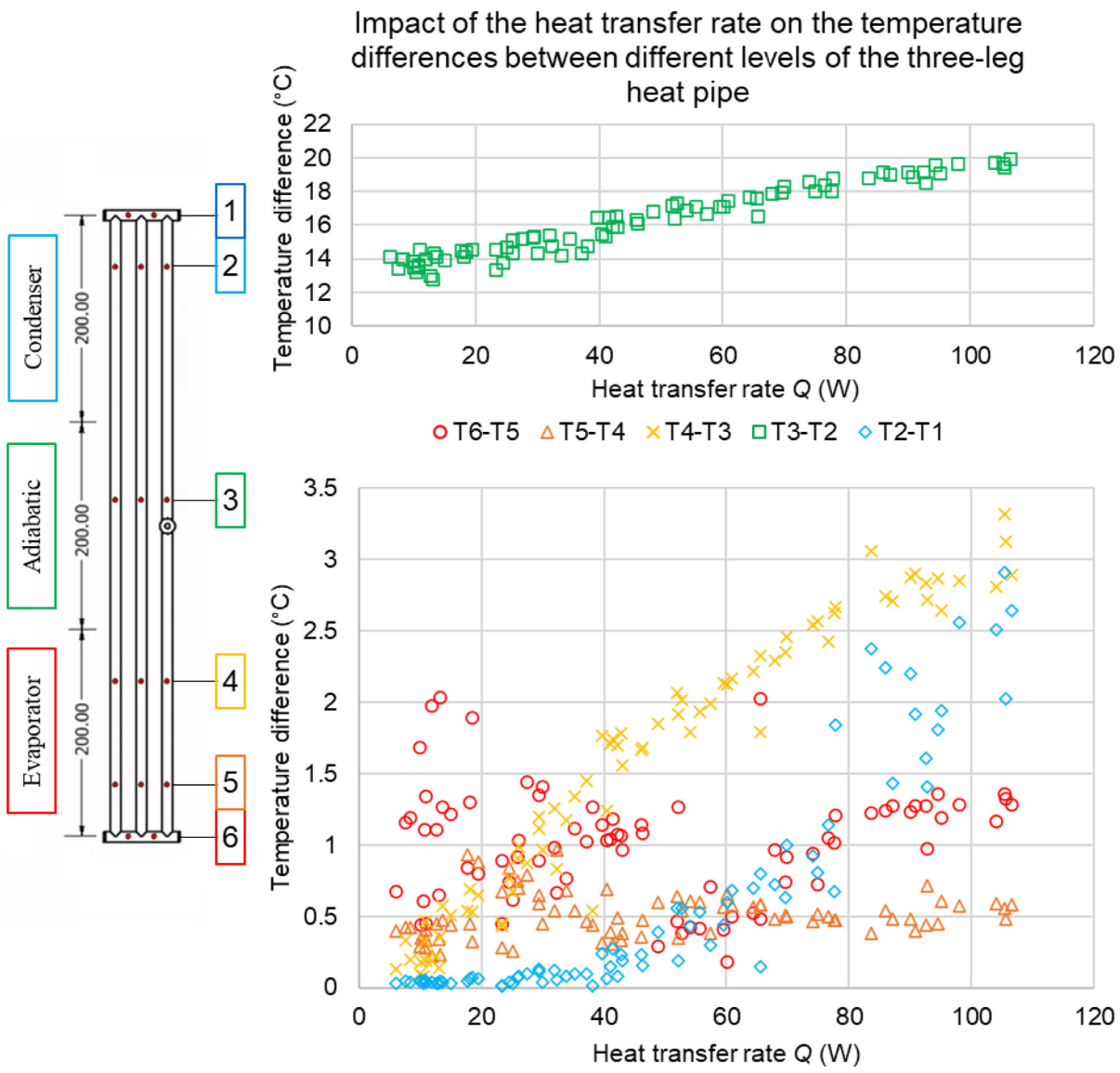

Fig. 13. Temperature differences between different levels of the three-leg heat pipe.

[8] model can be adjusted to suit experimental data. However, to date, the optimum value of condensation mass transfer coefficient for a given simulation cannot be predicted.

7.1.5. Conclusion on the CFD modelling of the three-leg heat pipe and limitations of the Lee model

In the conducted CFD modelling of the three-leg heat pipe, major limits of the commonly used Lee [8] model were identified. The impact of the three inputs of the Lee [8] model on the simulation of a three-leg heat pipe were studied: (1) the saturation temperature Tsat, (2) the evaporation mass transfer coefficient β_e, and (3) the condensation mass transfer coefficient β_c. A main issue of the Lee [8] model is that the values of the saturation temperature and mass transfer coefficients cannot be predicted. However, those inputs have a significant impact on the heat pipe simulation. In practice, the inputs of the Lee [8] model are usually adapted by researchers to suit the experimental data. In Fig. 12 is shown the typical temperature profile of a simulated heat pipe and how the three inputs of the Lee [8] model can be adjusted to fit with the experimental data.

At first, it was shown that the vapour temperature and temperature of the adiabatic section of the simulated heat pipe converge to the saturation temperature Tsat value provided. The simulated heat pipe temperature will then be centred around this value. Then, based on the mass transfer coefficients values, the temperature of the evaporator and condenser sections can be adapted. The evaporation mass transfer coefficient β_e can be modified to adjust the temperature of the simulated heat pipe evaporator. Similarly, the condensation mass transfer coefficient β_c can be changed to adjust the temperature of the condenser. As such, the currently available Lee [8] model cannot predict the temperatures of a heat pipe. In addition, the conducted simulations revealed that, in the Lee [8] model, the link between the mass transfer and heat transfer is poor. Indeed, for a similar mass transfer rate, it was shown that the temperature of the heat pipe can converge to different values which are dictated by the saturation temperature input given. Finally, the Lee [8] model treats both liquid and vapour phases separately which can lead to physical nonsense such as a vapour temperature higher than that of the saturated liquid pool. In this regards, the current Lee [8] is considered as unsuitable to numerically model heat pipes. It is believed that a turning point in the simulation of heat pipes must be taken by either modifying the Lee [8] model or using other multi-phase models.

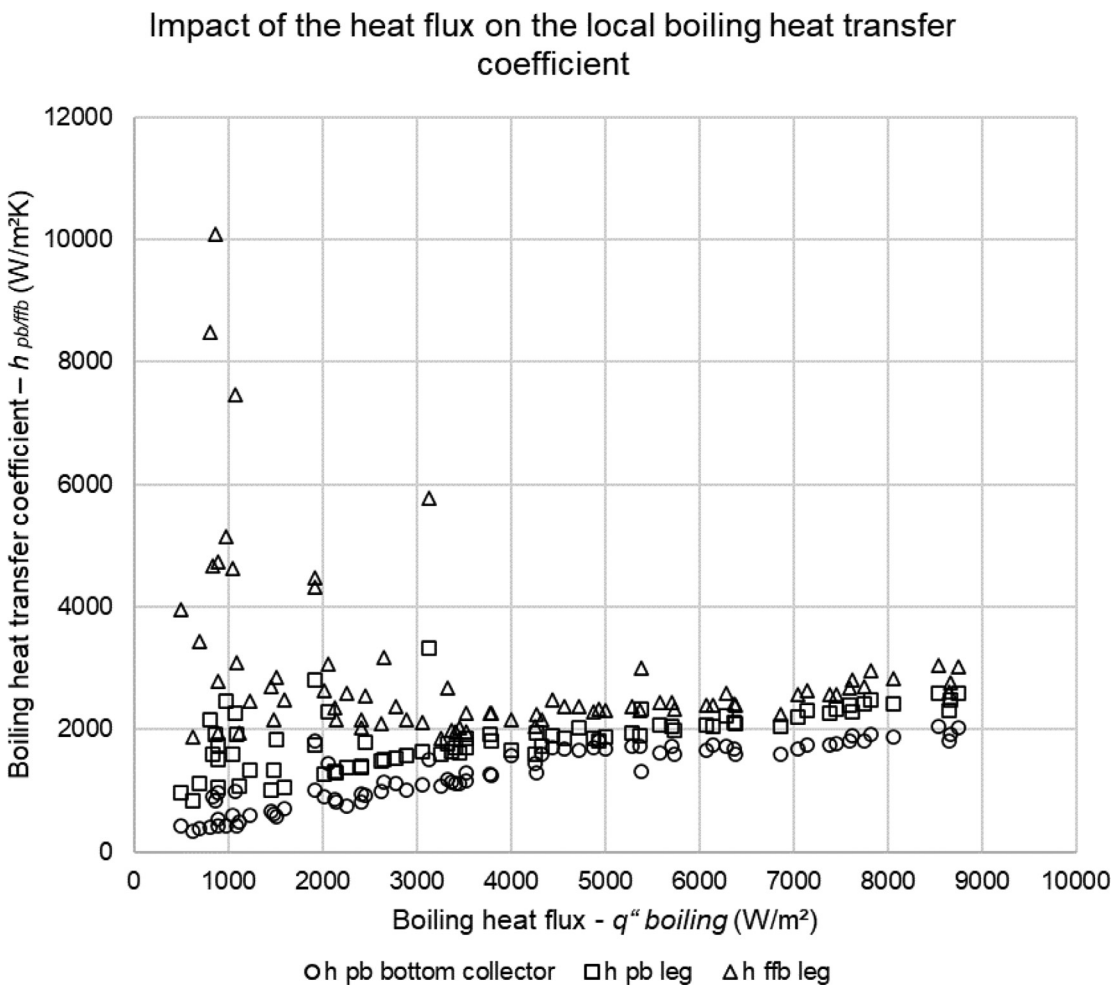

Fig. 14. Local heat transfer coefficients at the evaporator of the three-leg heat pipe.

Table 4
Heat transfer rate / heat flux conversion.

Heat transfer rate Q̇	0	20	40	60	80	100
Evaporator/ Condenser heat flux q″	0	1642.5	3284.9	4927.4	6569.9	8212.3

7.2. Theoretical model results

In this section, the theoretical modelling of the three-leg heat pipe is studied.

7.2.1. Thermal resistance model validation

By using the local temperature measurement from each leg and each collector of the three-leg heat pipe, the proposed multi-channel thermal resistance network was adapted and checked. By comparing the temperature difference between different sections of the three-leg heat pipe, the presence of a thermal resistance can be identified. The temperature differences between different levels of the three-leg heat pipe are presented in Fig. 13.

In Fig. 13, the results are displayed in terms of total heat transfer rate. However, those results could also be displayed in terms of heat flux at the evaporator or condenser. In the investigated three-leg heat pipe, both evaporator and condenser heat flux were similar. Table 4 shows the relation between the total heat transfer rate and the evaporator/condenser heat flux in the conducted experiment.

From Fig. 13 can be observed that the temperature difference between two sections of the heat pipe can increase with the heat transfer rate. For instance, between the level 2 of the three-leg heat pipe which is the condenser section and the level 3 which is the adiabatic section, the temperature difference increases with the heat transfer rate. This can be explained due to the presence of the condensation thermal resistance. In the case of the investigated three-leg heat pipe, due to the small diameter of the tubes and small heat transfer area, the condensation thermal resistance is very large which generates high temperature gradients. Nevertheless, the instantaneous rise of condenser temperature witnesses that the heat pipe operates normally. Hence, by studying the temperature difference between different levels of the heat pipe, the presence of a thermal resistance can be detected. At the bottom of the evaporator, with an increase of the heat transfer rate, the difference of temperature between the bottom collector (level 6) and the bottom section of the legs (level 5) is relatively constant. On average, the temperature of the bottom collector is about 1 °C higher than the legs. This temperature difference is relatively small and does not seem to indicate the presence of a thermal resistance between both sections of the three-leg heat pipe. Moreover, the temperature profile shows that pool boiling occurs in both bottom collector and in the legs. A similar observation can be made by studying the temperature difference between the levels 5 and 4.

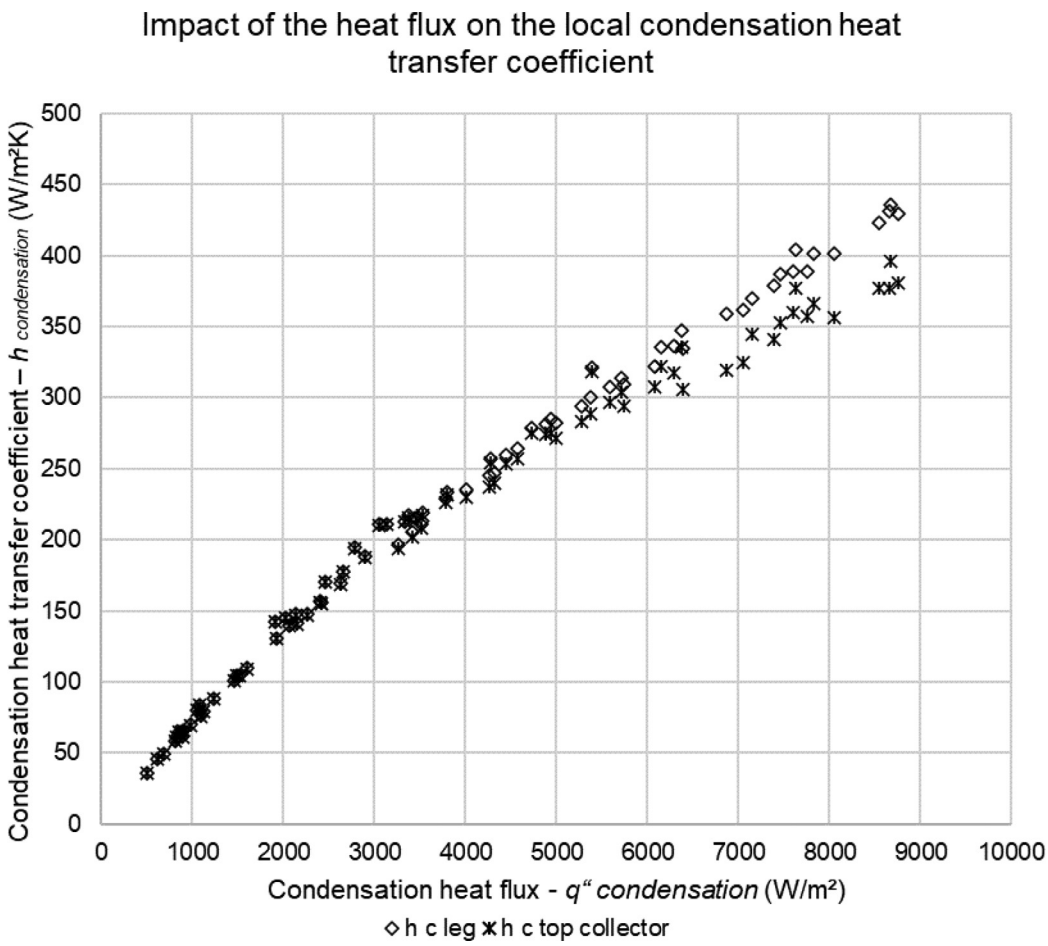

Fig. 15. Local heat transfer coefficients at the condenser of the three-leg heat pipe.

These represent the temperature at the evaporator section between the top section of the legs and the bottom. Again, this difference of temperature is found to be constant for all heat transfer rates. The temperature at the bottom of the legs is about 0.5 °C higher than the top of the legs. Surprisingly, the temperature measurements from the three-leg heat pipe shows that pool boiling took place at the top of the legs. It is assumed that an inacurate charging of the three-leg heat pipe led to a filing ratio of 100%. Moreover, the small temperature difference between the top and bottom of the legs indicates that a unique pool boiling thermal resistance can be considered for each leg. Obviously, between the adiabatic section (level 3) and the evaporator (level 4), the temperature difference increases with the heat transfer rate due to the presence of the boiling thermal resistance. More interestingly, at the condenser section, the temperature difference between the top collector (level 1) and the legs (level 2) increases with the heat transfer rate. This indicates that the temperature of the legs and top collector should not be considered uniform at the condenser section and that different thermal resistances should be considered. To complete the analysis of the three-leg heat pipe temperature profile and develop the multi-channel thermal resistance network, the local heat transfer coefficients were measured and studied. In Fig. 14 are studied the heat transfer coefficients at the evaporator of the three-leg heat pipe.

In Fig. 14, three local heat transfer coefficients taking place at the evaporator of the three-leg heat pipe are displayed. The pool boiling heat transfer coefficient of the bottom collector is shown with circular markers, the heat transfer coefficient at the bottom of the leg is shown with square markers, and the heat transfer coefficient at the top of the legs is shown with triangle markers. Over the whole range of boiling heat flux, it is observed that both heat transfer coefficients at the bottom collector and bottom of the legs are very close. Yet, the pool boiling heat transfer coefficient at the bottom of the legs is slightly higher than that of the bottom of the legs. To consider this small difference between the bottom collector and the legs, it is relevant to include different thermal resistances in the multi-channel thermal resistance network. Regarding the heat transfer coefficient at the top of the legs, at heat flux lower than 3500 W/m^2, some inacuracies in the measurements are detected. These could be due to the geyser boiling effect in the bottom cylinder or to the proximity of the thermocouples with the adiabatic section. Overall, the heat transfer coefficient at the top of the leg is slightly higher that that of the bottom of the leg. However, the difference is small. At heat flux higher than 3500W/m^2, the heat transfer coefficient at the top of the leg is more accurate and very close to the heat transfer coefficient measured at the bottom of the leg. This small difference indicates that the temperature of each parallel leg can be considered uniform and that a single thermal resistance for each leg can be used in the thermal resistance network.

Like the analysis made at the evaporator, Fig. 15 shows the local heat transfer coefficients measured at the condenser of the three-leg heat pipe.

In Fig. 15, the condensation heat transfer coefficient of the legs is displayed with diamonds markers whereas the top collector heat transfer coefficient is shown with cross markers. It is observed that both local heat transfer coefficients are very close. At condensation heat flux lower than 5500 W/m^2, no difference can be detected be-

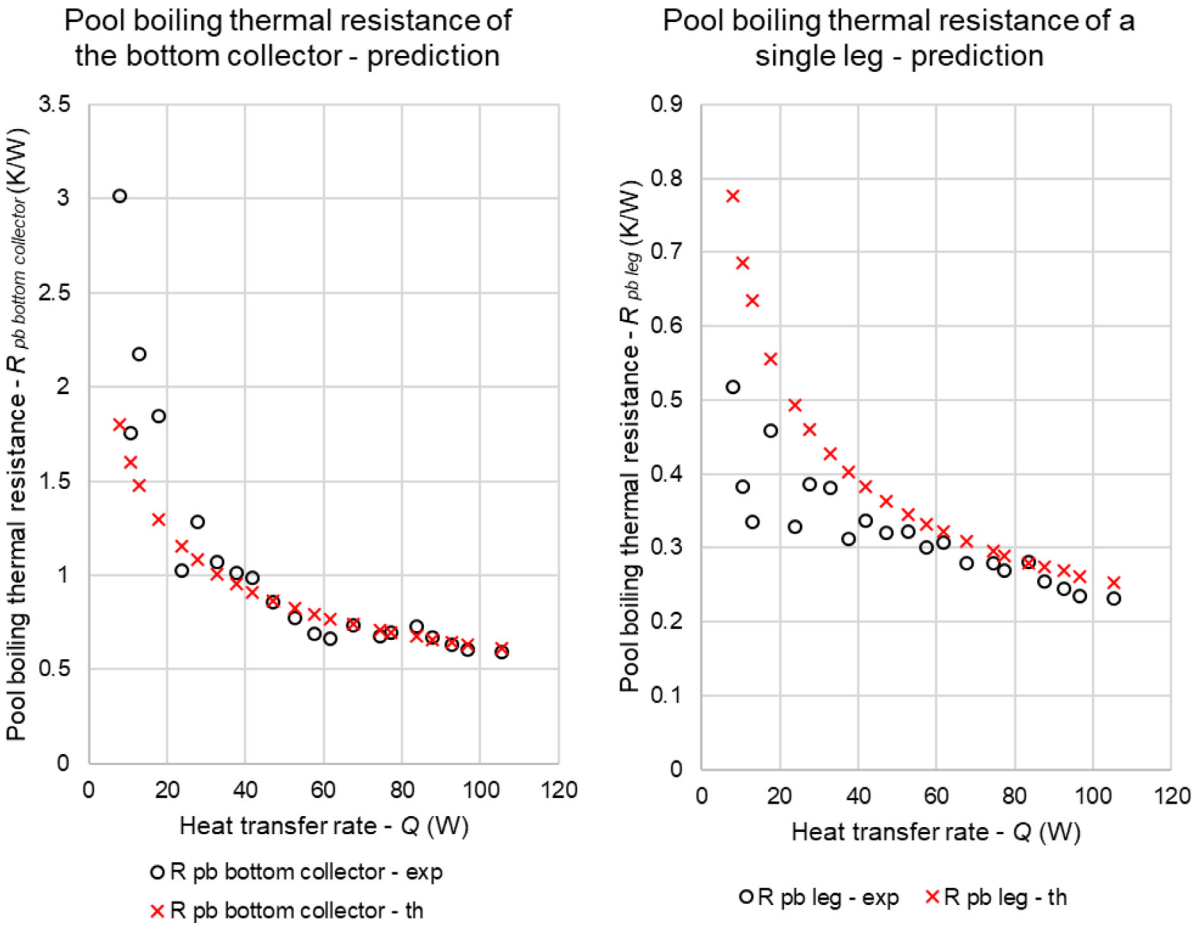

Fig. 16. Local pool boiling thermal resistances theoretical prediction.

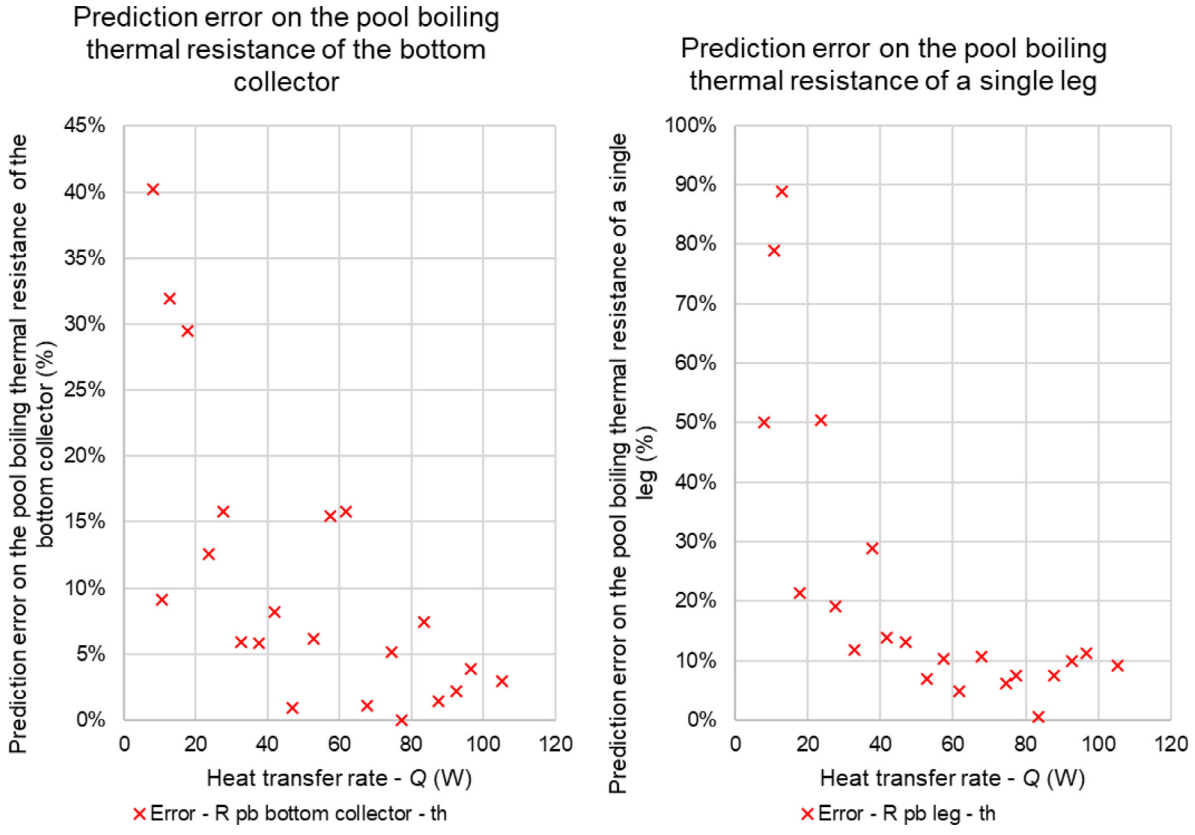

Fig. 17. Prediction error on the local pool boiling thermal resistances.

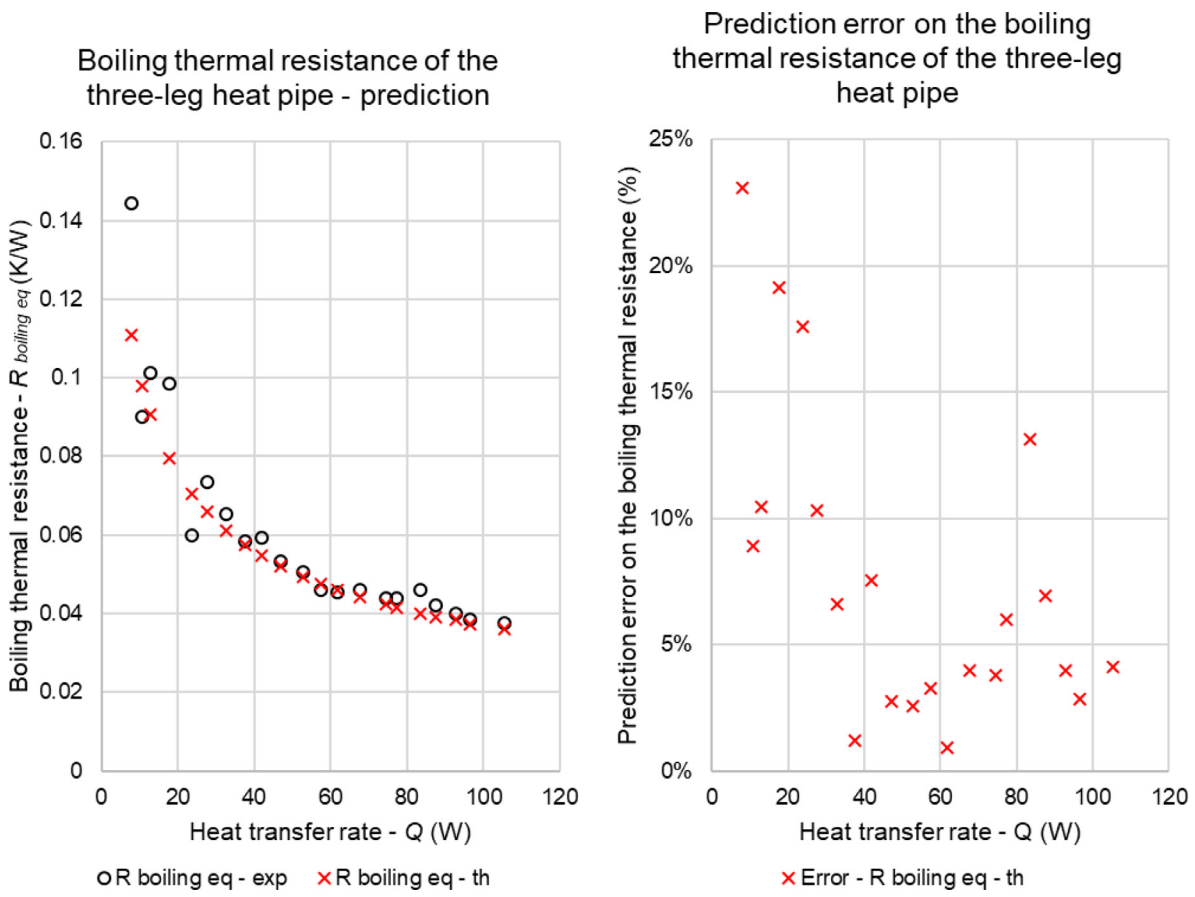

Fig. 18. Theoretical prediction of the boiling thermal resistance of the three-leg heat pipe.

tween both heat transfer coefficients. However, at heat flux higher than 5500 W/m^2, the leg heat transfer coefficient becomes higher than that of the top collector. This difference increases with the heat transfer rate. This phenomena is assumed to be caused by a different condensation pattern occuring in the horizontal collector. The horizontal orientation is expected to favor the accumulation of liquid condensate and the increase of the condensate thickness. As a result, at high heat transfer rate where the mass transfer rate is important, the condensation heat transfer coefficient in the horizontal top collector becomes lower than that of the vertical legs. It is therefore advised to consider different thermal resistances of condensation for the top collector and vertical legs. Based on those observations, the multi-channel thermal resistance network presented in Fig. 6 was developed.

7.2.2. Boiling thermal resistance prediction

To predict the local pool boiling thermal resistances of the three-leg heat pipe, pool boiling heat transfer coefficient correlations were selected. To predict the thermal resistance of the bottom collector, the correlation by Shiraishi et al. [48] was used. For the prediction of the pool boiling thermal resistance of each independent leg, the correlation from Imura et al. [49] was found more suitable. In Fig. 16 are shown the theoretical prediction of the local pool boiling thermal resistances of the three-leg heat pipe.

In Fig. 16 are displayed with circular black markers the experimental local pool boiling thermal resistances whereas the red crosses markers represent the theoretical predictions. The predictions of the local thermal resistances of pool boiling are directly related to the accuracy of the correlation chosen. For the bottom collector, the pool boiling thremal resistance is high at low heat transfer rates but decreases quickly. Indeed, at a heat transfer rate of 10W, the bottom collector pool boiling thermal resistance is about 2 K/W whereas, at a heat transfer rate of 50 W, this thermal resistance is down to 0.75 K/W. It is observed that, despite a slight underprediction of the pool boiling thermal resistance of the bottom collector, the correlation from Shiraishi et al. [48] remains very accurate over the whole range of heat transfer rates investigated. The experimental pool boiling heat transfer coefficient of the parallel legs is significantly lower than that of the bottom collector. Yet, the trend is similar and the pool boiling thermal resistance keeps decreasing with an increase of the heat transfer rate. This is explained by the higher bubble activity and the transition to a fully developed nucleate pool boiling regime [54]. It can be observed that the theoretical prediction of the pool boiling thermal resistance of each leg is less accurate than that of the bottom collector. The correlation from Imura et al. [49] tends to overpredict the pool boiling thermal resistance over the whole range of heat transfer rates. This error is higher at low heat transfer rates where the experimental error is high. However, from a heat transfer rate of 30W, the predictive error becomes reasonable. This can be better observed from Fig. 17 which shows the prediction error in percentage for both bottom collector and legs pool boiling thermal resistances theoretical predictions.

From the left-hand side of Fig. 17 is presented the prediction error made on the estimation of the bottom collector pool boiling thermal resistance. At small heat transfer rates, the predictive error is higher but remains acceptable and lower than 40%. However, from a heat transfer rate of 20W, most of the prediction samples show an error lower than 10%. The few predictive values which lead to an error higher than 10% are mainly due to experimental

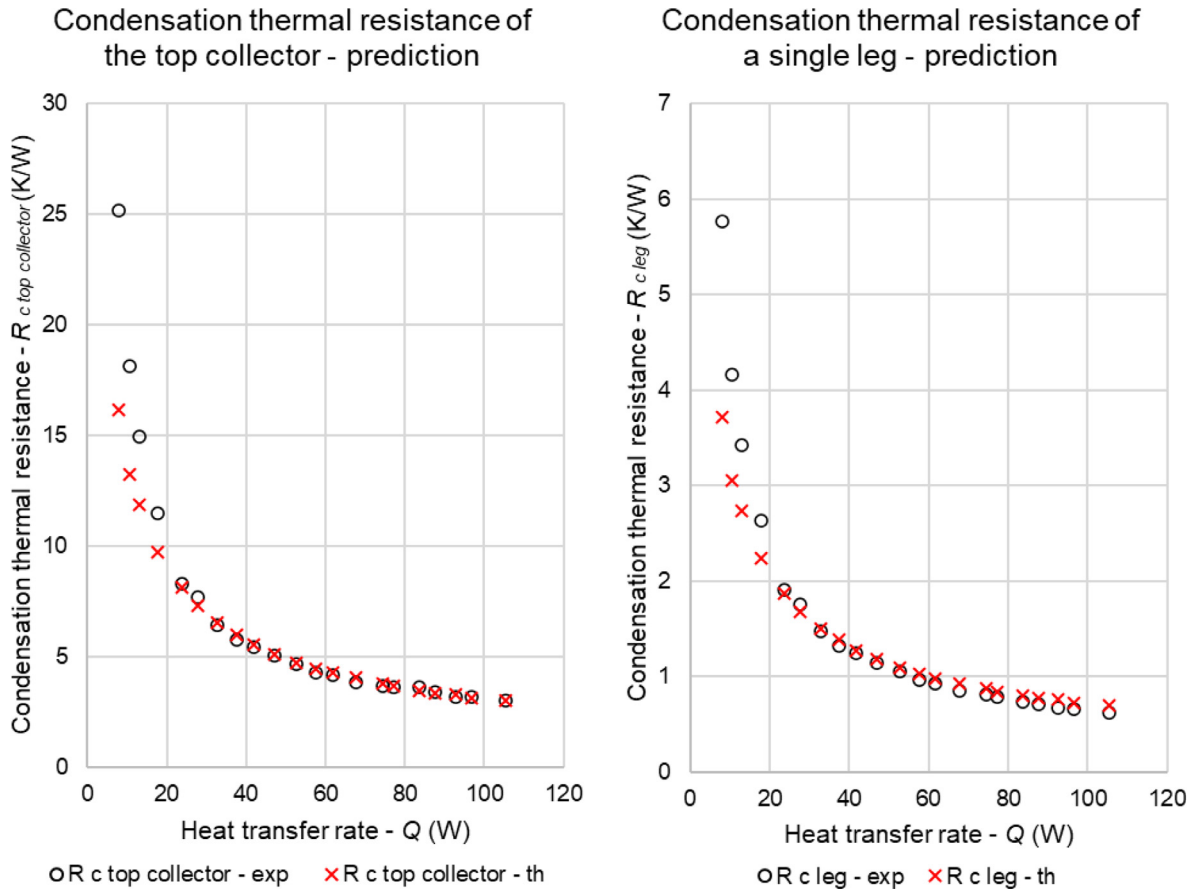

Fig. 19. Local condensation thermal resistances theoretical prediction.

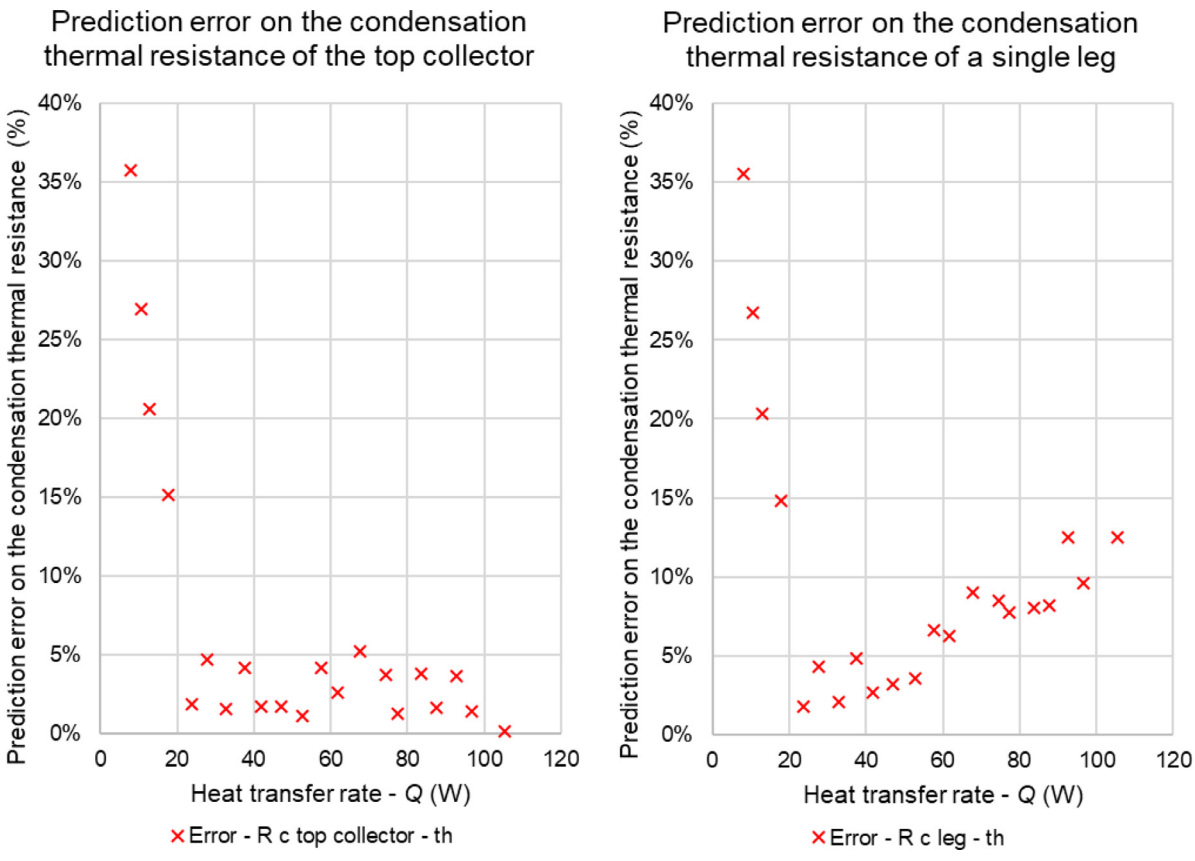

Fig. 20. Prediction error on the local condensation thermal resistances.

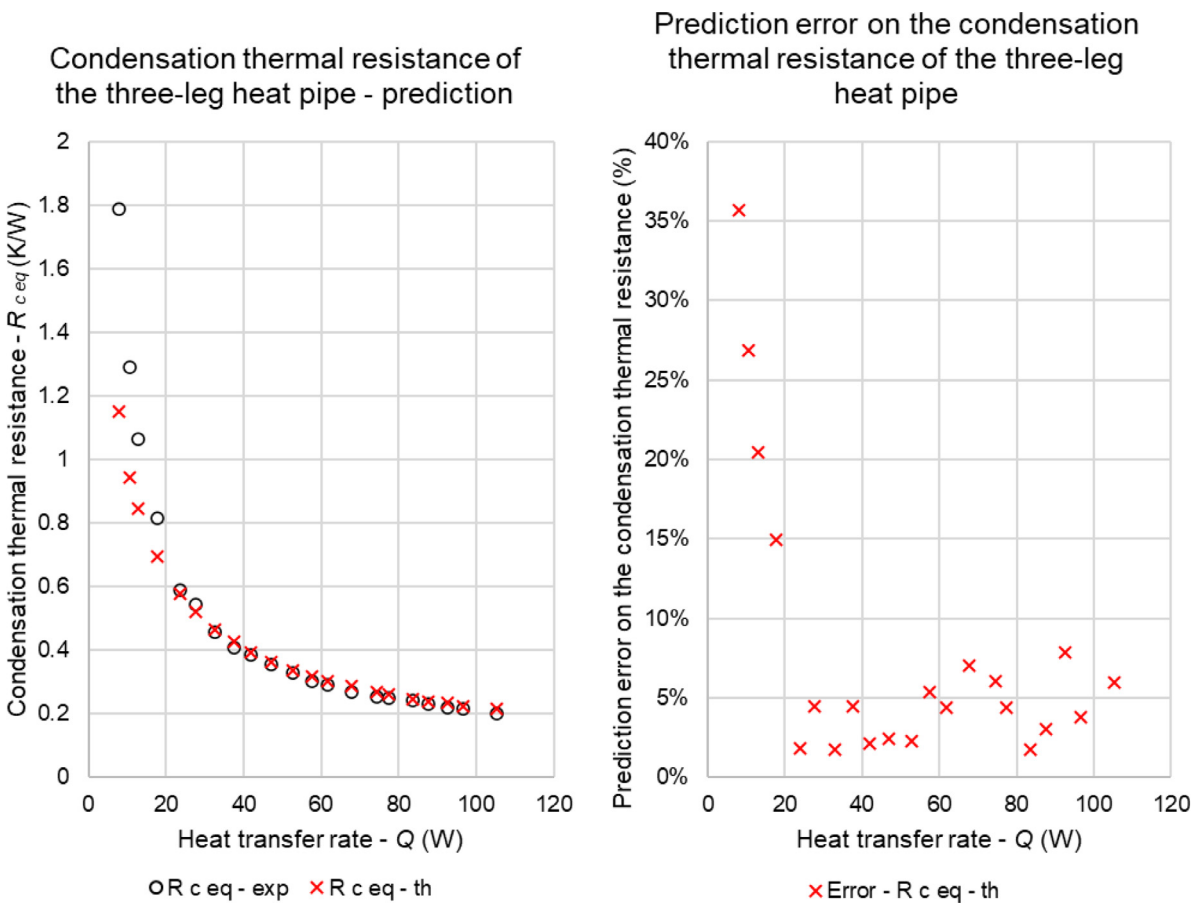

Fig. 21. Theoretical prediction of the condensation thermal resistance of the three-leg heat pipe.

inacuracies and fluctuations. For instance, at 60W, the prediction makes an error of 15% which, as witnesses Fig. 16, is due to experimental inacuracies. For the theoretical prediction of the legs, the inacuracies are more important at low heat transfer rates where the predictive error can be as high as 90%. This is due to an important overprediction of the pool boiling thermal resistance by the correlation from Imura et al. [49] at heat transfer rates lower than 20 W. Again, at higher heat transfer rates, the theoretical prediction and experimental data become closer. From a heat transfer rate of 40 W, the theoretical error becomes less than 15%. Based on the prediction of the local pool boiling thermal resistances of the bottom collector and parallel legs, the multi-channel thermal resistance network was used to predict the overall boiling thermal resistance of the three-leg heat pipe. The boiling thermal resistance prediction of the three-leg heat pipe is presented in Fig. 18.

On the left-hand side of Fig. 18 are shown the experimental and theoretical estimation of the boiling thermal resistance of the three-leg heat pipe whereas, on the right-hand side is shown the predictive error. By combining the local thermal resistances of the bottom collector and three parallel legs, the theoretical prediction of the boiling thermal resistance is found to be relatively accurate. Even at very low heat transfer rates where the experimental data are less accurate, the theoretical model was able to predict the boiling thermal resistance of the three-leg heat pipe within 25% of error. With an increase of the heat transfer rate, the theoretical model becomes more accurate. At heat transfer rates higher than 30 W, the prediction error is lower than 10%. Over the whole range of heat transfer rate investigated, the average error made on the prediction of the three-leg heat pipe boiling thermal resistance is 7.6%.

7.2.3. Condensation thermal resistance prediction

To predict the local condensation thermal resistances of the parallel legs and top collector, the correlation from Schnabel and Palen [50] was used and integrated to the multi-channel thermal resistance network. In Fig. 19 are presented the theoretical prediction of the top collector and single leg condensation thermal resistances.

In comparison to the pool boiling thermal resistances, the local condensation thermal resistances of the three-leg heat pipe are significantly higher. At a heat transfer rate of 10W, the top collector condensation thermal resistance is as high as 25K/W whereas that of the leg is 6K/W. The theoretical prediction in red reveals that the model is more accurate at medium and high heat transfer rates. At low heat transfer rate, the local condensation thermal resistances is underpredicted by the correlation from Schnabel and Palen [50]. Yet, from a heat transfer rate of 20 W, the prediction agrees better with the experimental data. For the top collector thermal resistance, the model remains accurate for all heat transfer rates in the range 20–110 W. However, at heat transfer rates higher than 70W, for the prediction of a single leg condensation thermal resistance, the correlation from Schnabel and Palen [50] leads to a slight overprediction. In Fig. 20, the prediction error made by the theoretical model on the local condensation thermal resistances is presented.

At low heat transfer rates, the predictive error is similar for both local condensation thermal resistances. At a heat transfer rate of 10 W, the prediction error is about 35% and decreases to 15% at 20 W. For the prediction of the top collector condensation thermal resistance, between a heat transfer rate of 20 W and 110 W, the prediction error from the theoretical model is small and remains

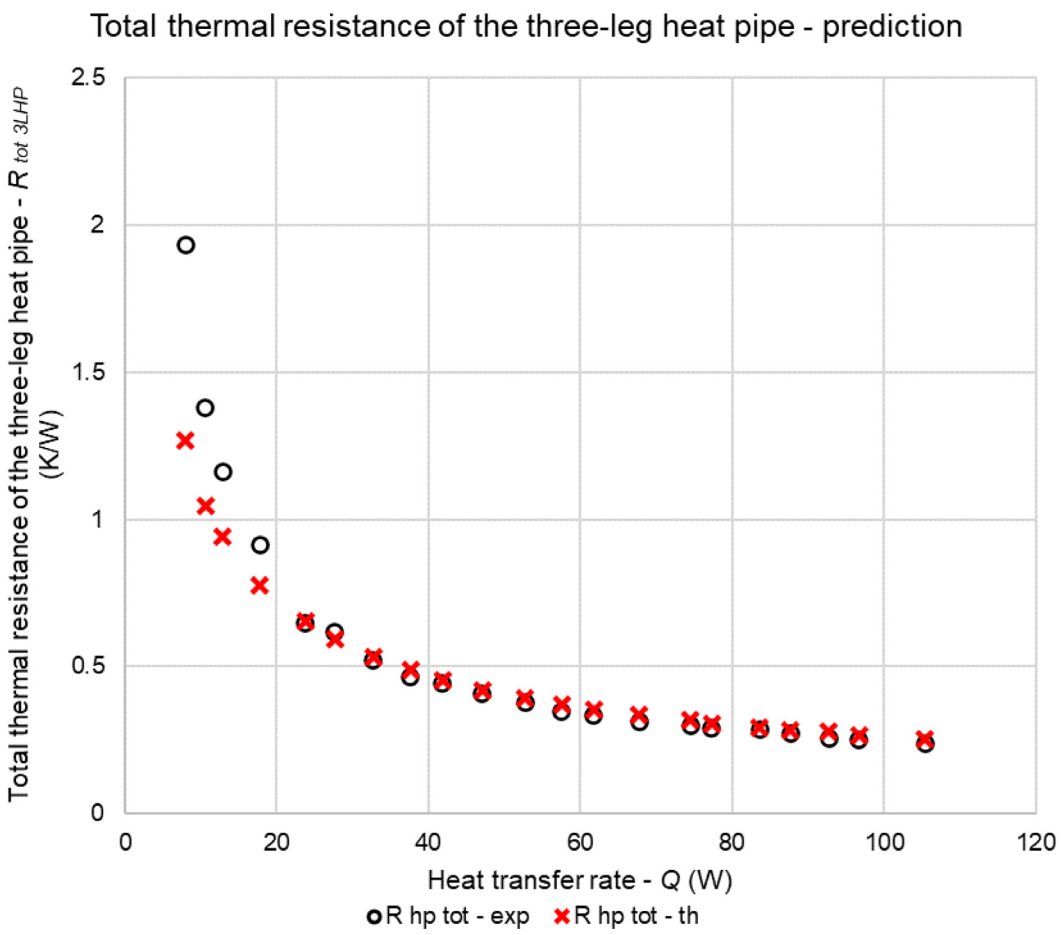

Fig. 22. Theoretical prediction of the total thermal resistance of the three-leg heat pipe.

lower than 5%. For the prediction of the single leg condensation thermal resistance, the error is minimum at 30 W and progressively increases with an increase of the heat transfer rate. However, in the range of heat transfer rates investigated, the predictive error remains acceptable and is below 15% at 110W. Based on the prediction of the local thermal resistance of condensation taking place in the parallel channels and top collector, the equivalent condensation thermal resistance of the three-leg heat pipe was predicted. To do so, the multi-channel thermal resistance network was used and the predictions presented in Fig. 21 were obtained.

Experimentally, the three-leg heat pipe condensation thermal resistance decreases with an increase of the heat transfer rate. At low heat transfer rates, the condensation thermal resistance of the three-leg heat pipe was about 1.8K/W, progressively decreases, and stabilizes around 0.2 K/W at 110 W. Regarding the theoretical prediction from the multi-channel heat pipe model, the accuracy of the prediction is less at low heat transfer rates. Indeed, the condensation thermal resistance is underpredicted at heat transfer rates lower than 20 W. As a result, the error made by the predictive model is 35% at 10 W but decreases quickly to 15% at 20 W. At heat transfer rates higher than 20 W, the prediction fits closely with the experimental data. Indeed, the predictive error remains lower than 10% for the prediction of the three-leg heat pipe condensation thermal resistance. Over the whole range of heat transfer rates investigated, the condensation thermal resistance of the three-leg heat pipe was predicted with an average error of 8.0%.

7.2.4. Total three-leg heat pipe thermal resistance prediction

By using the complete multi-channel thermal resistance network, the total thermal resistance of the three-leg heat pipe was estimated theoretically. This includes both boiling and condensation thermal resistances but also the radial and axial conduction thermal resistances. The prediction of the total thermal resistance of the three-leg heat pipe is presented in Fig. 22.

In Fig. 22, the experimental total thermal resistance of the three-leg heat pipe is shown with black circular markers whereas the theoretical prediction is displayed with red cross markers. Between 10 W and 110 W, the thermal resistance of the three-leg heat pipe undergoes an exponential-like decrease with an increase of the heat transfer rate. At low heat transfer rate, the total thermal resistance is maximum and up to 2 K/W. However, the total thermal resistance of the multi-channel heat pipe decreases to 1 K/W at 20 W and stabilizes around 0.25 K/W at a maximum heat transfer rate of 110 W. Regarding the theoretical prediction of the total thermal resistance of the three-leg heat pipe, the prediction of the condensation thermal resistance plays a significant role in the accuracy of the model. Indeed, the condensation thermal resistance represents 85% of the three-leg heat pipe total thermal resistance. In this regard, the prediction of the total thermal resistance of the three-leg heat pipe is close to that of the condensation thermal resistance. Again, the theoretical model is less accurate at low heat transfer rates. Indeed, below 20W, the total thermal resistance of the three-leg heat pipe is underpredicted. However, at heat transfer rates higher than 20W, the prediction from the theoretical model becomes more accurate. In Fig. 23 is presented the accuracy of the theoretical model regarding the prediction of the total thermal resistance of the three-leg heat pipe.

From a heat transfer rate of 8 W to 18 W, the error on the prediction decreases from 34% to 15%. With an increase of the heat transfer rate, the accuracy of the multi-channel heat pipe theoret-

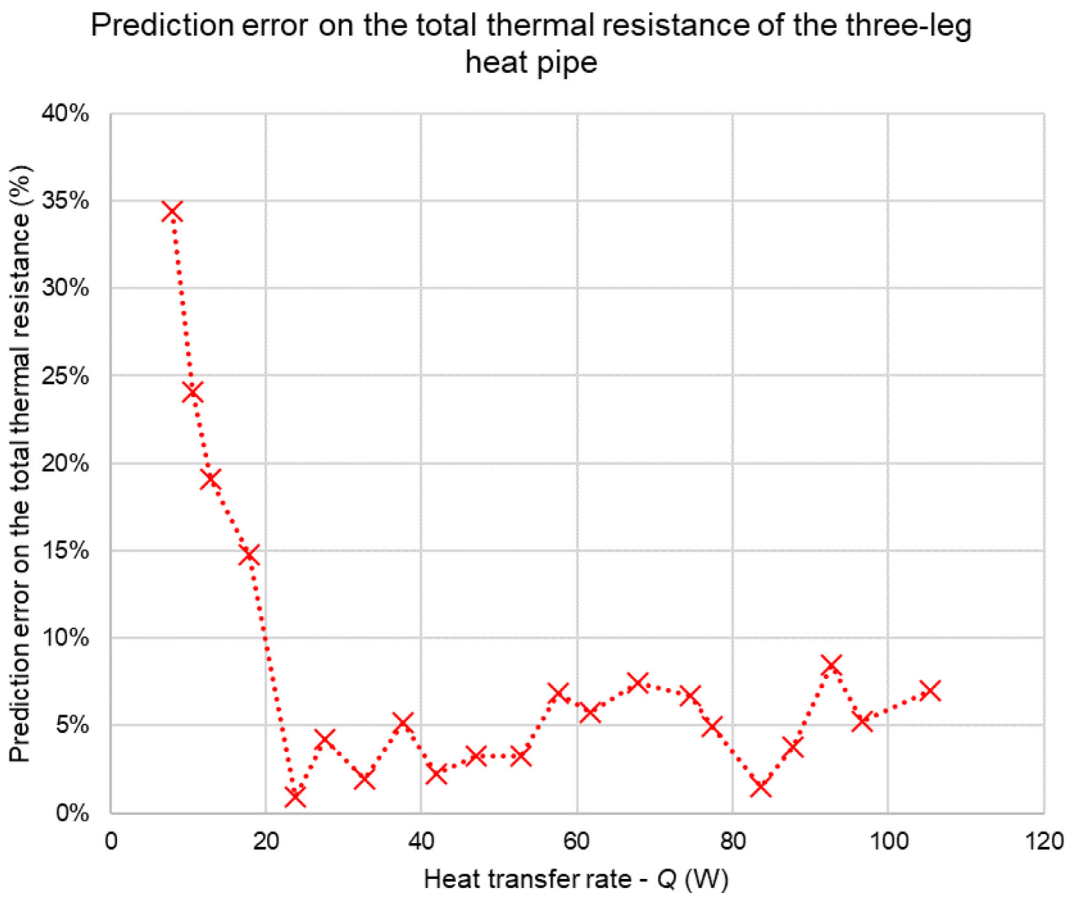

Fig. 23. Prediction error on the total thermal resistance of the three-leg heat pipe.

ical model is improved. As a result, at heat transfer rates higher than 20W, the predictions agree with the experimental data within 10%. The error made by the model is minimum at a heat transfer rate of 22W where the prediction curve crosses the experimental data. Then, at higher heat transfer rates, a slight overprediction of the single leg condensation thermal resistance leads to an increase of the theoretical model error. Nevertheless, even at high heat transfer rates where the condensation thermal resistance of a single leg was overpredicted, the prediction of the total thermal resistance of the three-leg heat pipe remains lower than 10%. Overall, the average error of the multi-channel heat pipe theoretical model obtained is 8.2%.

8. Conclusion

In this research, the numerical (CFD) and theoretical modelling of multi-channel heat pipes was addressed. To investigate the modelling of a multi-channel heat pipe, a unique and one of its kind three-leg heat pipe prototype was manufactured and used for the development of the models. This prototype permitted local temperature measurement to be taken from each parallel channel and both top and bottom collectors.

For the development of the numerical (CFD) model, the widely used Lee [8] model and Volume of Fluid approach was used. For the first time, the CFD modelling of the three-leg heat pipe permitted to identify major limits in the current Lee [8] model:

- The Lee [8] model saturation temperature input cannot be predicted by the numerical solver.
- The vapour temperature of the simulated heat pipe converges to the saturation temperature implemented.
- In the Lee [8] model, the liquid and vapour phases are treated separately which can lead to physical nonsense such as a vapour temperature much higher than that of the evaporating liquid pool.
- The link between the heat and mass transfer is poor and the mass transfer has little impact on the heat pipe temperatures simulated.
- The mass transfer coefficient needed in the Lee [8] model cannot be predicted by the Lee [8] model and are usually adapted.

To date, by changing the value of saturation temperature and mass transfer coefficients, the Lee [8] model is usually adapted to suit experimental data. It is therefore concluded that the Lee [8] model is currently unable to predict the performance of a heat pipe using CFD and that a turning point should be taken in the numerical simulation of heat pipes. For future work regarding the CFD modelling of heat pipes, other multi-phase models should be considered or the current Lee [8] model needs to be adapted. It would also be beneficial to develop a time independent two-phase model which does not need iteration to update the liquid and vapour source term. This would allow steady state CFD simulations of heat pipes to be conducted.

Regarding the theoretical model of the three-leg heat pipe, the local temperature measurement taken from the legs and collectors permitted the development and validation of a new multi-channel heat pipe thermal resistance network. The local heat transfer coefficients revealed that different two-phase mechanisms can take place in the horizontal collectors and can lead to significantly different heat transfer coefficient compared to the parallel channels. In this regard, it seems relevant to consider different thermal resistances for the horizontal collectors. By integrating the suit-

able two-phase correlations, the boiling and condensation thermal resistances of the three-leg heat pipe prototype were predicted within an average error of 7.6%, 8.0%. Over a heat transfer rate range of 10–110 W, the multi-channel heat pipe theoretical model was able to predict the total thermal resistance of the three-leg heat pipe with an average error of 8.2%.

Declaration of Competing Interest

We wish to confirm that there are no known conflicts of interest associated with this publication and there has been no financial support for this work that could have influenced its outcome.

We confirm that the manuscript has been read and approved by all named authors and that there are no other persons who satisfied the criteria for authorship but are not listed. We further confirm that the order of authors listed in the manuscript has been approved by all of us.

We confirm that we have given due consideration to the protection of intellectual property associated with this work and that there are no impediments to publication, including the timing of publication, with respect to intellectual property. In so doing we confirm that we have followed the regulations of our institutions concerning intellectual property.

We understand that the Corresponding Author is the sole contact for the Editorial process (including Editorial Manager and direct communications with the office). He is responsible for communicating with the other authors about progress, submissions of revisions and final approval of proofs. We confirm that we have provided a current, correct email address which is accessible by the Corresponding Author and which has been configured to accept email from the IJHMT Journal.

Signed by all authors as follows:

Professor Hussam Jouhara (On behalf of the co-authors)
25/11/2022

CRediT authorship contribution statement

Valentin Guichet: Conceptualization, Methodology, Writing – original draft, Writing – review & editing. **Bertrand Delpech:** Conceptualization, Methodology, Writing – review & editing. **Hussam Jouhara:** Conceptualization, Methodology, Writing – original draft, Writing – review & editing.

Data availability

Data will be made available on request.

Acknowledgments

The research presented in this paper has received funding from the European Union's H2020 Programme ETEKINA and iWAYS under grant agreement numbers 768772 and 958274, respectively.

References

[1] H. Jouhara, et al., The performance of a novel flat heat pipe based thermal and PV/T (photovoltaic and thermal systems) solar collector that can be used as an energy-active building envelope material, Energy 108 (2016) 148–154 Aug., doi:10.1016/J.ENERGY.2015.07.063.
[2] H. Jouhara, et al., The performance of a heat pipe based solar PV/T roof collector and its potential contribution in district heating applications, Energy 136 (2017) 117–125 Oct, doi:10.1016/J.ENERGY.2016.04.070.
[3] H. Jouhara, et al., Heat pipe based battery thermal management: evaluating the potential of two novel battery pack integrations, Int. J. Thermofluids 12 (2021) 100115 Nov, doi:10.1016/J.IJFT.2021.100115.
[4] H. Jouhara, N. Serey, N. Khordehgah, R. Bennett, S. Almahmoud, S.P. Lester, Investigation, development and experimental analyses of a heat pipe based battery thermal management system, Int. J. Thermofluids 1 (2020) 100004 –2Feb, doi:10.1016/J.IJFT.2019.100004.
[5] A.G. Olabi, et al., Battery thermal management systems: recent progress and challenges, Int. J. Thermofluids 15 (2022) 100171 Aug, doi:10.1016/J.IJFT.2022.100171.
[6] H. Jouhara, "Waste heat recovery in process industries," Waste Heat Recover. Process Ind., Mar. 2022, doi:10.1002/9783527830008.
[7] R.W. Schrage, A Theoretical Study of Interphase Mass Transfer, Columbia University Press, 1953.
[8] W.H. Lee, Pressure iteration scheme for two-phase flow modeling." *IN" MULTIPHASE TRANSPORT: FUNDAMENTALS, REACTOR SAFETY*, APPLICATIONS" (1980) 407–432.
[9] X. Wang, Y. Zhu, Y. Wang, Development of pressure-based phase change model for CFD modelling of heat pipes, Int. J. Heat Mass Transf. 145 (2019) 118763 Dec, doi:10.1016/j.ijheatmasstransfer.2019.118763.
[10] B.A. Nichita, J.R. Thome, A level set method and a heat transfer model implemented into FLUENT for modeling of microscale two phase flows, in: Proceedings of the AVT-178 Specialists' Meeting on System Level Thermal Management for Enhanced Platform Efficiency, 2010 CONF.
[11] J. Legierski, B. Wie¸cek, G. de Mey, Measurements and simulations of transient characteristics of heat pipes, Microelectron. Reliab. 46 (1) (2006) 109–115 Jan, doi:10.1016/J.MICROREL.2005.06.003.
[12] M. Knudsen, The Kinetic Theory of Gases, Methuen & Co. Ltd, London, 1934.
[13] A.A.B. Temimy, A.A. Abdulrasool, CFD modelling for flow and heat transfer in a closed thermosyphon charged with water-a new observation for the two phase interaction, IOP Conf. Ser. Mater. Sci. Eng. 518 (3) (2019), doi:10.1088/1757-899X/518/3/032053.
[14] X. Wang, et al., CFD modeling of liquid-metal heat pipe and hydrogen inactivation simulation, Int. J. Heat Mass Transf. 199 (2022) 123490 Dec, doi:10.1016/J.IJHEATMASSTRANSFER.2022.123490.
[15] H. Sun, et al., CFD simulation based on film model of high temperature potassium heat pipe at different positions: Horizontal, vertical, and 45° inclined, Prog. Nucl. Energy 154 (2022) 104442 Dec, doi:10.1016/J.PNUCENE.2022.104442.
[16] A. Alizadehdakhel, M. Rahimi, A.A. Alsairafi, CFD modeling of flow and heat transfer in a thermosyphon, Int. Commun. Heat Mass Transf. 37 (3) (2010) 312–318 Mar, doi:10.1016/J.ICHEATMASSTRANSFER.2009.09.002.
[17] Z. Lin, S. Wang, R. Shirakashi, L.W Zhang, Simulation of a miniature oscillating heat pipe in bottom heating mode using CFD with unsteady modeling, Int. J. Heat Mass Transf. 57 (2) (2013) 642–656 Feb, doi:10.1016/J.IJHEATMASSTRANSFER.2012.09.007.
[18] K. Kafeel, A. Turan, Axi-symmetric simulation of a two phase vertical thermosyphon using Eulerian two-fluid methodology, Heat Mass Transf. 49 (8) (2013) 1089–1099 und Stoffuebertragung, doi:10.1007/s00231-013-1155-6.
[19] K. Kafeel, A. Turan, Simulation of the response of a thermosyphon under pulsed heat input conditions, Int. J. Therm. Sci. 80 (2014) 33–40 Jun, doi:10.1016/J.IJTHERMALSCI.2014.01.020.
[20] L. Asmaie, M. Haghshenasfard, A. Mehrabani-Zeinabad, M. Nasr Esfahany, Thermal performance analysis of nanofluids in a thermosyphon heat pipe using CFD modeling, Heat Mass Transf. 49 (5) (2013) 667–678 und Stoffuebertragung, doi:10.1007/s00231-013-1110-6.
[21] B. Fadhl, L.C. Wrobel, H. Jouhara, CFD modelling of a two-phase closed thermosyphon charged with R134a and R404a, Appl. Therm. Eng. 78 (2015) 482–490 Mar, doi:10.1016/J.APPLTHERMALENG.2014.12.062.
[22] Y. Kim, J. Choi, S. Kim, Y. Zhang, Effects of mass transfer time relaxation parameters on condensation in a thermosyphon, J. Mech. Sci. Technol. 29 (12) (2015) 5497–5505, doi:10.1007/s12206-015-1151-5.
[23] Y. Wang, et al., CFD simulation of an intermediate temperature, two-phase loop thermosiphon for use as a linear solar receiver, Appl. Energy 207 (2017) 36–44 Dec, doi:10.1016/J.APENERGY.2017.05.168.
[24] C. Yue, Q. Zhang, Z. Zhai, L. Ling, CFD simulation on the heat transfer and flow characteristics of a microchannel separate heat pipe under different filling ratios, Appl. Therm. Eng. 139 (2018) 25–34 Jul, doi:10.1016/j.applthermaleng.2018.01.011.
[25] K. Hosseinzadeh, D.D. Ganji, F. Ommi, Effect of SiO2 super-hydrophobic coating and self-rewetting fluid on two phase closed thermosyphon heat transfer characteristics: An experimental and numerical study, J. Mol. Liq. 315 (2020) 113748 Oct, doi:10.1016/j.molliq.2020.113748.
[26] W.W. Wang, Y. Cai, L. Wang, C.W. Liu, F.Y. Zhao, D. Liu, Thermo-hydrodynamic analytical model, numerical solution and experimental validation of a radial heat pipe with internally finned condenser applied for building heat recovery units, Energy Convers. Manag. 219 (2020) 113041 Sep, doi:10.1016/j.enconman.2020.113041.
[27] A. Wei, X. Ren, S. Lin, X. Zhang, CFD analysis on flow and heat transfer mechanism of a microchannel Ω-shape heat pipe under zero gravity condition, Int. J. Heat Mass Transf. 163 (2020) 120448 Dec, doi:10.1016/J.IJHEATMASSTRANSFER.2020.120448.
[28] A. Tarokh, C. Bliss, A. Hemmati, Performance enhancement of a two-phase closed thermosyphon with a vortex generator, Appl. Therm. Eng. 182 (2021) 116092 Jan, doi:10.1016/j.applthermaleng.2020.116092.
[29] S. Zimmermann, M. Klippel, R. Dreiling, T. Nguyen-Xuan, M. Pfitzner, A volume-of-fluid heat pipe model resolving pressure discontinuities at the wick-vapor interface, Int. J. Heat Mass Transf. 194 (2022) 123100 Sep, doi:10.1016/J.IJHEATMASSTRANSFER.2022.123100.

[30] B. Fadhl, L.C. Wrobel, H. Jouhara, Numerical modelling of the temperature distribution in a two-phase closed thermosyphon, Appl. Therm. Eng. 60 (1–2) (Oct. 2013) 122–131, doi:10.1016/J.APPLTHERMALENG.2013.06.044.
[31] Z.H. Liu, Y.Y. Li, R. Bao, Thermal performance of inclined grooved heat pipes using nanofluids, Int. J. Therm. Sci. 49 (9) (2010) 1680–1687 Sep, doi:10.1016/j.ijthermalsci.2010.03.006.
[32] S.D. Fertahi, T. Bouhal, Y. Agrouaz, T. Kousksou, T. El Rhafiki, Y. Zeraouli, Performance optimization of a two-phase closed thermosyphon through CFD numerical simulations, Appl. Therm. Eng. 128 (2018) 551–563 Jan, doi:10.1016/J.APPLTHERMALENG.2017.09.049.
[33] T. Höhne, CFD simulation of a heat pipe using the homogeneous model, Int. J. Thermofluids 15 (2022) 100163 Aug, doi:10.1016/J.IJFT.2022.100163.
[34] S. Almahmoud, H. Jouhara, Experimental and theoretical investigation on a radiative flat heat pipe heat exchanger, Energy 174 (2019) 972–984 May, doi:10.1016/J.ENERGY.2019.03.027.
[35] S. Almahmoud, "Experimental and theoretical investigation on a radiative flat heat pipe heat exchanger for waste recovery in the steel industry," PhD Thesis, Brunel University London, UK, 2019.
[36] B. Delpech, B. Axcell, H. Jouhara, Experimental investigation of a radiative heat pipe for waste heat recovery in a ceramics kiln, Energy 170 (2019) 636–651 Mar, doi:10.1016/J.ENERGY.2018.12.133.
[37] V. Guichet, N. Khordehgah, H. Jouhara, Experimental investigation and analytical prediction of a multi-channel flat heat pipe thermal performance, Int. J. Thermofluids (2020) 100038 Jul, doi:10.1016/j.ijft.2020.100038.
[38] V. Guichet, B. Delpech, N. Khordehgah, H. Jouhara, Experimental and theoretical investigation of the influence of heat transfer rate on the thermal performance of a multi-channel flat heat pipe, Energy 250 (2022) 123804 Jul, doi:10.1016/J.ENERGY.2022.123804.
[39] H. Jouhara, B. Fadhl, L.C. Wrobel, Three-dimensional CFD simulation of geyser boiling in a two-phase closed thermosyphon, Int. J. Hydrog. Energy 41 (37) (2016) 16463–16476 Oct, doi:10.1016/J.IJHYDENE.2016.02.038.
[40] B. Fadhl, "Modelling of the thermal behaviour of a two-phase closed thermosyphon," PhD Thesis, Brunel University London, UK, 2015.
[41] P.J. Linstrom, W.G. Mallard, The NIST chemistry WebBook: a chemical data resource on the internet, J. Chem. Eng. Data 46 (5) (2001) 1059–1063.
[42] "ANSYS FLUENT 12.0/12.1 Documentation." https://www.afs.enea.it/project/neptunius/docs/fluent/index.htm (weblink, accessed Mar. 14, 2022).
[43] S.C.K. De Schepper, G.J. Heynderickx, G.B. Marin, Modeling the evaporation of a hydrocarbon feedstock in the convection section of a steam cracker, Comput. Chem. Eng. 33 (1) (2009) 122–132 Jan, doi:10.1016/J.COMPCHEMENG.2008.07.013.
[44] S.C.K. De Schepper, G.J. Heynderickx, G.B. Marin, CFD modeling of all gas–liquid and vapor–liquid flow regimes predicted by the Baker chart, Chem. Eng. J. 138 (1) (2008) 349–357 –3May, doi:10.1016/J.CEJ.2007.06.007.
[45] W.M. Rohsenow, A method of correlating heat-transfer data for surface boiling of liquids, Trans. ASME. 74 (6) (Aug 1952) 969–975.
[46] ESDU 81038, Heat pipes - performances of two-phase closed thermosyphons, no, ESDU international plc, London, 1983.
[47] Y.A. Cengel, in: Heat Transfer: A Practical Approach, New York McGraw-Hill, 2003, pp. 785–841, doi:10.1017/CBO9781107415324.004.
[48] M. Shiraishi, K. Kikuchi, T. Yamanishi, Investigation of heat transfer characteristics of a two-phase closed thermosyphon, J. Heat Recovery Syst. 1 (4) (Jan. 1981) 287–297, doi:10.1016/0198-7593(81)90039-4.
[49] H. Imura, H. Kusuda, J.I. Ogata, T. Miyazaki, N. Sakamoto, Heat transfer in two-phase closed-type thermosyphons, JSME Trans. 45 (1979) 712–722.
[50] G. Schnabel, J.W. Palen, Wärmeubergang an Senkrechten Berieselten Flächen, Springer-Verlag Sect. Md., Berlin, 1998.
[51] H.I. Mohammed, D. Giddings, G.S. Walker, CFD multiphase modelling of the acetone condensation and evaporation process in a horizontal circular tube, Int. J. Heat Mass Transf. 134 (2019) 1159–1170 May, doi:10.1016/j.ijheatmasstransfer.2019.02.062.
[52] Z. Yang, X.F. Peng, P. Ye, Numerical and experimental investigation of two phase flow during boiling in a coiled tube, Int. J. Heat Mass Transf. 51 (5–6) (2008) 1003–1016 Mar, doi:10.1016/J.IJHEATMASSTRANSFER.2007.05.025.
[53] K. Goodson, A. Rogacs, M. David, C. Fang, Volume of fluid simulation of boiling two-phase flow in a vapor-venting microchannel, Front. Heat Mass Transf. 1 (1) (2010).
[54] V. Guichet, S. Almahmoud, H. Jouhara, Nucleate pool boiling heat transfer in wickless heat pipes (two-phase closed thermosyphons): a critical review of correlations, Therm. Sci. Eng. Prog. 13 (2019), doi:10.1016/j.tsep.2019.100384.